INVESTIGATING TRIM ALGORITHMS FOR A UTILITY HELICOPTER

A THESIS SUBMITTED TO
THE GRADUATE SCHOOL OF NATURAL AND APPLIED SCIENCES
OF
MIDDLE EAST TECHNICAL UNIVERSITY

BY

ANIL DEMİREL

IN PARTIAL FULFILLMENT OF THE REQUIREMENTS
FOR
THE DEGREE OF MASTER OF SCIENCE
IN
AEROSPACE ENGINEERING

NOVEMBER 2019

Approval of the thesis:

INVESTIGATING TRIM ALGORITHMS FOR A UTILITY HELICOPTER

submitted by **ANIL DEMİREL** in partial fulfillment of the requirements for the degree of **Master of Science in Aerospace Engineering Department, Middle East Technical University** by,

Prof. Dr. Halil Kalıpçılar
Dean, Graduate School of **Natural and Applied Sciences** _____

Prof. Dr. İsmail Hakkı Tuncer
Head of Department, **Aerospace Engineering** _____

Assoc. Prof. Dr. İlkay Yavrucuk
Supervisor, **Aerospace Engineering, METU** _____

Examining Committee Members:

Prof. Dr. Ozan Tekinalp
Aerospace Engineering, METU _____

Assoc. Prof. Dr. İlkay Yavrucuk
Aerospace Engineering, METU _____

Assoc. Prof. Dr. Nilay Sezer Uzol
Aerospace Engineering, METU _____

Assist. Prof. Dr. Ali Türker Kutay
Aerospace Engineering, METU _____

Assist. Prof. Dr. Yakup Sabri Özkazanç
Electrical and Electronics Engineering, HU _____

Date: 28.11.2019

I hereby declare that all information in this document has been obtained and presented in accordance with academic rules and ethical conduct. I also declare that, as required by these rules and conduct, I have fully cited and referenced all material and results that are not original to this work.

Name, Surname: Anıl Demirel

Signature:

ABSTRACT

INVESTIGATING TRIM ALGORITHMS FOR A UTILITY HELICOPTER

Demirel, Anıl
Master of Science, Aerospace Engineering
Supervisor: Assoc. Prof. Dr. İlkay Yavrucuk

November 2019, 94 pages

Obtaining trim positions of an aircraft is an issue of importance. In this thesis, the aim is to develop a procedure that can achieve the trim points with reasonable assumptions for the entire flight of a helicopter. In order to achieve this goal an autopilot is used to determine the trim points. A high-fidelity flight model is used. The structure is based on GENHEL model. Helicopter trim states are calculated for specified flight conditions. The parameters that are sensitive to trim convergence are determined. A simplified set of trim equations are solved to generate a proper input set for fast convergence of Nelder-Mead (NM) Simplex runs. A NM Simplex algorithm is used to find accurate trim points.

The procedure is tested for the UH-60 helicopter model in hover and forward flight conditions. A comparison of the trim results with flight test data available in literature is used to. Thereby the utility of the procedure is demonstrated, the reliability of the assumptions and the practicality of the model are shown.

Keywords: Helicopter, Trim, Simplex, GENHEL, Autopilot

ÖZ

GENEL MAKSAT HELİKOPTERİ İÇİN DENGE ALGORİTMALARININ İNCELENMESİ

Demirel, Anıl
Yüksek Lisans, Havacılık ve Uzay Mühendisliği
Tez Danışmanı: Doç. Dr. İlkay Yavrucuk

Kasım 2019, 94 sayfa

Hava aracını denge şartlarını belirlemek önem arz eden bir konudur. Bu çalışmada helikopterler için bütün uçuş zarfını kapsayan makul varsayımlar yaparak denge noktaları bulan bir prosedür geliştirmek hedeflendi. Bu hedefe ulaşmak için oto pilot ile birlikte model çalıştırılarak hedef denge noktaları bulundu. GENHEL modelini temel alan yüksek sadakate sahip bir model kullanıldı. Helikopterin denge durumları özel uçuş koşullarında bulunmuştur. Denge noktası için başlangıç değerleri önemli olan parametrelere karar verilmiştir. Doğru denge noktaları bulabilmek için Nelder-Mead (NM) Simplex yöntemi kullanılmıştır. Bu yöntemin daha çabuk yakınsamasını sağlamak için basitleştirilmiş denge denklemleri çözülerek daha uygun ilk değerler belirlenmiştir.

Geliştirilen prosedür UH-60 helikopter modeli ile değişik uçuş koşulları için test edildi. Elde edilen denge noktaları literatürde yer alan uçuş testler ile karşılaştırıldı. Bu sayede prosedürün geçerliliği onaylandı. Yapılan varsayımların güvenilirliği ve modelin kullanışlılığı doğrulandı.

Anahtar Kelimeler: Helikopter, Denge, Simplex, GENHEL, Oto Pilot

To my family…

ACKNOWLEDGEMENTS

First, I would like to express my sincere gratitude to Assoc. Prof. Dr. İlkay Yavrucuk for his encouragement and supervision throughout my studies.

I want to emphasize my special thanks to Prof. Dr. Demet Gülen for her continuous support and encouragement throughout the study.

I would also like to thank to my old company HAVELSAN for supporting.

I wish to state my thanks to my mother, Eren, and my brother, V. Emre, for their encouragement and patience.

Finally, I would like to express my deepest thanks to my wife Mrs. Zehra Demirel for her support, encouragement, patience and understanding.

TABLE OF CONTENTS

LIST OF TABLES

TABLES

LIST OF FIGURES

FIGURES

LIST OF SYMBOLS

BL	Distance in buttline station
C_L	Lift coefficient
C_D	Drag coefficient
C_y	Segment chord
F_P	Aero force of blade section, perpendicular to the blade span axes
F_T	Aero force of blade section, tangent to the blade span axes
F_{XA}, F_{YA}, F_{ZA}	Aero forces of blade in shaft axes
FS	Distance in fuselage station
I_θ	Shaft inclination angle
$I_\emptyset$	Shaft tilt angle
L, M, N	Rotor moments in body axes
M_{FAB}, M_{LAB}	Aero moments about hinge-blade span axis
NBS	Number of blades simulated
NM	Nelder-Mead
NSS	Number of blade segments simulated
Q	Torque, Dynamic pressure
R_T	Rotor Radius
S	Area
STE	Simplified trim equations
T, H, J	Total force components
U_P	Air velocity of blade section, perpendicular to the blade span axes

U_T	Air velocity of blade section, tangent to the blade span axes
U_{Y_I}	Total velocity in blade span axes
V_{Xb}, V_{Yb}, V_{Zb}	Body axes velocities
WL	Distance in waterline station
X, Y, Z	Rotor forces in body axes
b	Number of rotor blades
b_s	Number of blades simulated
e	Normalized offset
p, q, r	Body axes angular rates
ρ	Air density
y_2	Distance from hinge to segment midpoint
α	Angle of attack
β	Flapping angle, Sideslip angle
$\dot{\beta}$	Flapping rate
$\ddot{\beta}$	Flapping acceleration
β_0	Cone angle
β_{1C}	Longitudinal cone angle
β_{1S}	Lateral cone angle
Γ_{TR}	Tail rotor cant angle
δ	Lagging angle
θ	Blade pitch angle
θ_0	Collective pitch angle
θ_{1C}	Lateral cyclic pitch
θ_{1S}	Longitudinal cyclic pitch

θ_{FP}	Flight path angle
θ_t	Blade twist
λ	Inflow ratio
ϕ	Roll angle
ψ	Rotor azimuth position
Ω	Rotor shaft speed

Subscripts:

B	Body axes
BDSH	Body to shaft axes
BS	Blade span axes
CGB	CG of body
H	Hub axes
HT	Horizontal tail
I	Indicating from 1 to total segments number
IB	Indicating from 1 to simulated blade number
IS	Indicating from 1 to simulated blade segment number
MR	Main rotor
S	Shaft axes
SHBD	Shaft to body axes
TR	Tail rotor
VT	Vertical tail
w	Weight coefficient
WF	Fuselage

CHAPTER 1

INTRODUCTION

Finding trim conditions for a high-fidelity helicopter model is a topic of interest due to its non-linear behavior. For example, in a flight simulator a trimming function is often used. For higher quality training, obtaining more precise trim points in a short time period is critical. Starting the helicopter in a trimmed position from the desired point and reposing the helicopter to the intended conditions are significant for providing training at a targeted level. Also, helicopter trim computation is an important matter for also analyzing helicopter flight dynamics and stability. A reliable trim result is a crucial foundation for analyzing and evaluating the helicopter's flight quality. In addition, automatic flight control systems are designed and evaluated at trim conditions. Different models of aircraft are compared by using their trim conditions. Also, models are compared with flight data according at trim points.

Trim state and control input values are combined to set the total forces and moments acting on the helicopter to zero at a flight condition at that time. Since the helicopters are coupled multi-body vehicles, the trim equations are complex, higher-order and nonlinear with a large number of states. Therefore, it is a challenge to find trim conditions. One needs to use a highly efficient algorithm which can converge to the target value. The prediction of trim settings is still a demanding exercise taking into consideration the divergence of iterative schemes and excessive computing effort.

In 1981, in order to perform an engineering simulation for performance and handling qualities evaluations, J.J. Howlett of Sikorsky issued a NASA Contractor Report regarding a UH-60A Black Hawk engineering simulation program, which was a project for the US Army [1]. This study is taken as the basis for the helicopter model

that is developed in this thesis. A trim method is published in 1981 for this model [2]. It is based on adjusting two angles (sideslip and angle of attack) and four channels pilot inputs based on the deviations between the actual and the zero of the translational and rotational accelerations of the aircraft. Several different methods are used for further studies. The 1995-article by Peters and Barwey [3] is still a key reference for an extensive review of theory and traditional methods of trim. The main ones of these methods are Harmonic Balance, Guess Control, Periodic Shooting, Finite Elements in time and Auto Pilot methods.

The harmonic balance trim method is one of the earlier techniques available to obtain the forced response of nonlinear differential equations with periodic coefficients. The first study of harmonic balance trim to rotorcraft analysis was aimed to find the trim solution to a gyroplane rotor in autorotation [4]. The method was extended to improve the efficiency in the analysis of larger systems having many coupled degrees of freedom in later studies [5] [6]. Another method of finding trim is to guess control. Time is let run until transient decays, and the trim-constraint error is checked. A Newton method is applied to update the controls iteratively [7].

The third method is the periodic shooting method that is based on the linear system theory for periodic systems. This method finds the solution to differential equations with periodic coefficients [8] [9]. Achar and Gaonkar investigated parallel and serial periodic shooting with optimally damped Newton iterations [10]. This approach is taken in order to determine sensitivity to initial conditions. Periodic shooting can become time consuming for systems having a higher number of states in the model. Peters and Peters developed a discrete control method that extended its ability to systems with large number of states, including hidden states [11].

A fourth strategy is finite-element trim in time which is similar to periodic shooting method [12] [13]. In this method, the periodic solution of the nonlinear rotor equations was formulated by a direct analytical approach with a finite-element method in time.

Afterwards the trim conditions are calculated iteratively using a modified Newton method.

Using Autopilot is another method to find trim conditions. Autopilot trim supplements the system of equations with a control law. This law closes the loop between the flight condition and the trim control. The controller drives the system towards the target trim condition as the equations are integrated in time. The autopilot trim method was established by Peters, Kim and Chen [14]. In this method the rotor is trimmed using a simulated feedback controller that continuously adjusts the controls to achieve the desired forces and moments. Peters, Bayly and Li extended that work to develop a hybrid autopilot method [15] which combined the advantages of the periodic shooting method, the auto-pilot method and the discrete auto-pilot method.

Robust method and [16] dynamic neural networks [17] [18] were used for trim results in 2000s. Studies of neural networks focused on developing a trim network, a critical element required for successful direct neural dynamic programming designs. Also, hybrid generic algorithm is used in more recent studies [19] [20]. These are based on combining the particular advantages of the traditional numerical and modern genetic algorithms effectively. The genetic algorithm can converge quickly in the initial stage and the traditional numerical algorithm can converge rapidly in local part.

This thesis describes the implementation of a MATLAB based computational tool that allows numerical trimming of complex high-fidelity simulation models in SIMULINK. The trim points are determined by using iteration, Nelder-Mead (NM) Simplex and Autopilot methods. A comparative discussion of the trim points found by three different methods is provided.

In this thesis, the generic helicopter developed at HAVELSAN is used. GENHEL [1] is used as a source document for aerodynamic block and FCS block data. AFCS block is tuned for UH-60 helicopter. By using this autopilot, trim points are calculated.

Since, autopilot should be tuned after each design change. Normally, design of an autopilot should start at trim points. In the scope of this thesis, a procedure is developed to obtain the trim points without using autopilot.

For this purpose, a script is used to estimate initial conditions for the NM Simplex search algorithm. The initial condition are estimated using simplified trim equations. It is executed in MATLAB to obtain the trim points. These trim points are used as the initial condition of NM Simplex method. At the final step a script is developed to enable a compatible execution of trim point calculations using the SIMULINK UH-60 helicopter model and "fminsearch" command of MATLAB through which the trim points are refined by using NM Simplex method.

In Chapter 2 models used for nonlinear helicopter simulation are presented. Chapter 3 gives the details of trim theory and trim algorithm development methodology. Chapter 4 presents simulation results of the automatic flight control system. Finally, conclusions are given.
Work done in this thesis:

- A helicopter model which is based on GENHEL document is tuned for this thesis,
- Trim point is found with AFCS,
- Trim point is found with the procedure developed,
- Three trim points found by two different methods are compared with Flight data.

CHAPTER 2

HELICOPTER MODELING

A high-fidelity helicopter model developed by HAVELSAN is used as a base model for this thesis. In order to be independent from software infrastructure of HAVELSAN, sub-blocks of MATLAB are used for environment and equation of motion models. GENHEL [1] is used as a source for the modifications of main rotor, tail rotor and flight control system. In addition to autopilot model is tuned for UH-60.

The main framework is developed in MATLAB & SIMULINK environment. Model components are developed in C++ and used as a library in MATLAB & SIMULINK. The main diagrams for helicopter dynamic model are presented in Figures 2.1 and 2.2. Pilot commands are taken as input by dynamic model. Flight gear program is used in order to visualize the model output.

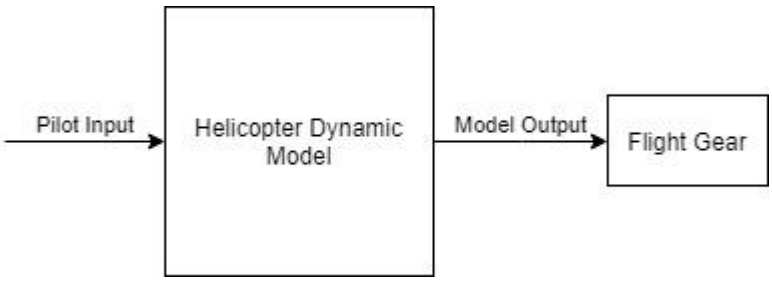

Figure 2.1. Generic helicopter model block diagram representation

Figure 2.2. Helicopter dynamic model block diagram representation

Environment Model, Flight Control System (FCS) and Automatic Flight Control System (AFCS), Weight and Balance (WAB), Ground Handling, Aerodynamics and 6-DOF (Degree of Freedom) Equations of Motion (EOM) are the model [figure 2.2].

Environment block calculates temperature, air pressure and air density. Aerodynamics block include main and tail rotor, fuselage and horizontal and vertical tail sub-models. The general structure of aerodynamics block models is based on reference [1]. FCS and AFCS blocks include flight control system, stability augmentation system (SAS) and autopilot modes such as altitude hold, air speed hold. Ground handling model includes landing gear and ground interaction computations. WAB block includes moment of inertia, total weight calculations and determination of center of gravity (CG) location. Translational and rotational accelerations, velocities and positions are calculated from total forces and moments affecting on the helicopter in different flight regimes by EOM block.

List of required models in a rotary wing simulation includes main and tail rotor, control systems, landing gear, fuselage, engines, horizontal and vertical tail and mutual interference effects and atmosphere [21]. Because of no ground start or

landing/take-off, landing gear model is not performed in thesis. Also, there is an ideal engine model, thus the required torque is used as generated torque.

2.1. Aerodynamic Model

Aerodynamic model consists of four subsystems which are main rotor, tail rotor, fuselage and empennage. Reference [1] is used as the source of aerodynamic data and model. It is a model source which is used widely in literature [22-24]. It is validated with flight data of UH-60. The block diagram of the model is given Figure 2.3.

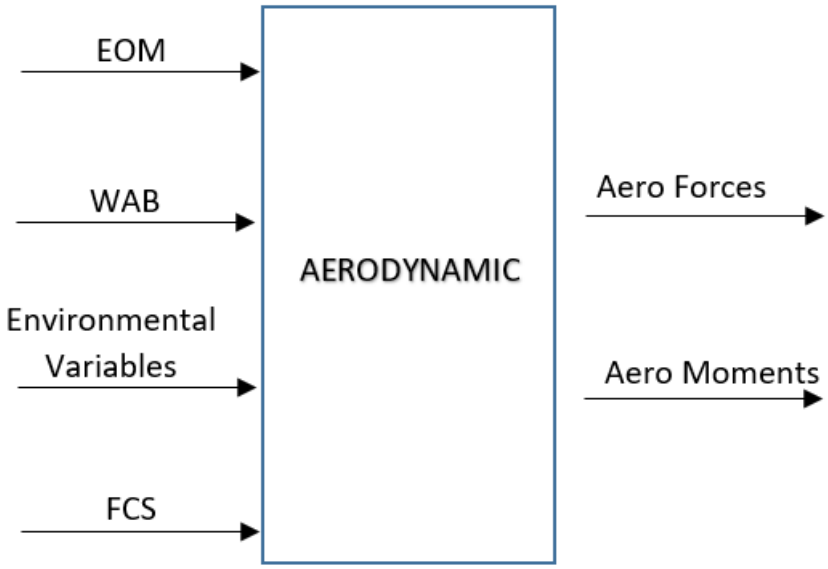

Figure 2.3. Schematic representation of aerodynamic block

The aerodynamic block gets inputs from EOM, WAB, Environment and FCS blocks. In the following table, inputs of aerodynamic model are listed. The inputs are detailed in the related subsystems.

Table 2.1. *Description of aerodynamic model input*

Variable Name:	**Parameter Name:**	**Description:**
EOM	u_dot	Acceleration along X-axis
	v_dot	Acceleration along Y-axis
	w_dot	Acceleration along Z-axis
	p	Angular rate about X-axis
	q	Angular rate about Y-axis
	r	Angular rate about Z-axis
	p_dot	Angular acceleration about X-
	q_dot	Angular acceleration about Y-
	r_dot	Angular acceleration about Z-
	phi	Body roll degree of freedom
	theta	Body pitch degree of freedom
	psi	Body yaw degree of freedom
	Altitude	Altitude
	u	Velocity along X-axis
	v	Velocity along Y-axis
	w	Velocity along Z-axis
Environmental Variables	g	Gravity
	Speedofsound,	Speed of sound
	rho	Density
FCS	Thetas	Blade pitch angles
WAB	Pos_Aero_CG	CG positions of parts

The model gives aerodynamic forces and aerodynamic moments as outputs. The subsystems are detailed below.

2.1.1. Main Rotor Model

There are various ways to model a helicopter main rotor. Same approaches are Perturbation Models, Rotor Disc Models, Rotor Blade Map Models, and Rotor Blade Element Models [25].

Blade Element Rotor Model (BERM) is used for main rotor simulation. This model calculates the forces on each blade element due to its motion through the air and hence the performance of the entire rotor. It is assumed that each blade element acts as a two-dimensional airfoil section producing aerodynamic forces which are the numerically integrated along the blade span. Virtual blades that are distributed through equal azimuth angle intervals over the rotor disk area are constructed to obtain more realistic solution results. The virtual blades are divided into small sections (segments) from root to the tip of the blade. The detailed description and formulation can be found on related books [26] [27]. The UH-60 helicopter has four blades. In calculations, eight virtual blades are added. Thus, total number of blades is twelve. Blades are located on a circular disc at 30^0 intervals. The dynamic inflow model of Pitt and Peters [28] [29] are used in this thesis.

Force and moment equations about the hub fixed shaft axes are given below. Further information about the parameters in the equations can be found in Appendix A.

$$T_H = -\frac{b}{b_s}\sum_{IB=1}^{NBS} F_{ZA_{IB}} \tag{2.1}$$

$$H_H = \frac{b}{b_s}\sum_{IB=1}^{NBS}\left\{F_{YA_{IB}}\cos(\psi_{IB}) - F_{XA_{IB}}\sin(\psi_{IB})\right\} \tag{2.2}$$

$$J_H = -\frac{b}{b_s}\sum_{IB=1}^{NBS}\left\{F_{XA_{IB}}\cos(\psi_{IB}) - F_{YA_{IB}}\sin(\psi_{IB})\right\} \tag{2.3}$$

$$M_H = \frac{b}{b_s} \sum_{IB=1}^{NBS} e * F_{ZA_{IB}} * \cos(\psi_{IB}) \tag{2.4}$$

$$L_H = \frac{b}{b_s} \sum_{IB=1}^{NBS} e * F_{ZA_{IB}} * \sin(\psi_{IB}) \tag{2.5}$$

$$Q_H = -\frac{b}{b_s} \sum_{IB=1}^{NBS} \left\{ e * F_{XA_{IB}} - M_{LAB_{IB}} \cos(\beta_{IB}) \right\} \tag{2.6}$$

where "b" is total number of blades and "b_s" is the number of azimuthally separated locations. ψ is the blade azimuth angle. NBS stands for the total number of blades. Body to shaft axes transformation matrix is

$$A_{BDSH} = \begin{bmatrix} \cos I_\theta & 0 & -\sin I_\theta \\ \sin I_\theta \sin I_\emptyset & \cos I_\emptyset & \cos I_\theta \sin I_\emptyset \\ \sin I_\theta \cos I_\emptyset & -\sin I_\emptyset & \cos I_\theta \cos I_\emptyset \end{bmatrix} \tag{2.7}$$

$$[A_{SHBD}] = [A_{BDSH}]^T \tag{2.8}$$

where $I_\emptyset$ is shaft tilt angles and I_θ is the shaft inclination angles.

These forces and moment about the hub fixed shaft axes are transformed to body axes and forces are transferred to center of gravity of helicopter.

$$\begin{bmatrix} X_{MR} \\ Y_{MR} \\ Z_{MR} \end{bmatrix} = A_{SHBD} \begin{bmatrix} -H_H \\ -J_H \\ -T_H \end{bmatrix} \tag{2.9}$$

$$\begin{bmatrix} L_{MR} \\ M_{MR} \\ N_{MR} \end{bmatrix} = A_{SHBD} \begin{bmatrix} L_H \\ M_H \\ Q_H \end{bmatrix} + \begin{bmatrix} Y_H Z_{MR} - Z_H Y_{MR} \\ Z_H X_{MR} - X_H Z_{MR} \\ X_H Y_{MR} - Y_H X_{MR} \end{bmatrix} \tag{2.10}$$

where X_H , Y_H , Z_H are longitudinal, lateral and vertical rotor arms from the CG of the aircraft.

2.1.2. Tail Rotor Model

Tail rotor model is based on reference [1]. Tail rotor model mathematical formulations are given below. The tail rotor is modeled as Bailey rotor Ref [2]. The forces and moments of tail rotor at the CG in body axes are obtained;

$$X_{TR} = -\frac{1}{2}\rho C_{D_{TR}} V_{XTR}{}^2 \tag{2.11}$$

$$Y_{TR} = T_{TR}\sin\Gamma_{TR} \tag{2.12}$$

$$Z_{TR} = -T_{TR}\cos\Gamma_{TR} \tag{2.13}$$

$$L_{TR} = Y_{TR}W_{TR} - Z_{TR}B_{TR} \tag{2.14}$$

$$M_{TR} = Z_{TR}F_{TR} - X_{TR}W_{TR} + \theta_{TR}\sin(\Gamma_{TR}) \tag{2.15}$$

$$N_{TR} = X_{TR}B_{TR} - Y_{TR}F_{TR} - \theta_{TR}\cos(\Gamma_{TR}) \tag{2.16}$$

2.1.3. Fuselage Model

Fuselages of helicopters have arbitrary geometric shapes generally. Since it is hard to develop high-fidelity fuselage mathematical model without aerodynamic coefficient tables. In this study, to develop higher fidelity model, Blackhawk fuselage aerodynamic force and moment coefficient tables in reference [1] are used. Fuselage model is based on reference [1] and the equations are given below.

Fuselage forces and moments in wind axis are determined by;

$$D_{FUS} = DQFTOT * Q_{WF} \tag{2.17}$$

$$Y_{FUS} = YQFTOT * Q_{WF} \tag{2.18}$$

$$L_{FUS} = LQFTOT * Q_{WF} \tag{2.19}$$

$$R_{FUS} = RQFTOT * Q_{WF} \tag{2.20}$$

$$M_{FUS} = MQFTOT * Q_{WF} \tag{2.21}$$

$$N_{FUS} = NQFTOT * Q_{WF} \tag{2.22}$$

DQFTOT, YQFTOT, LQFTOT, RQFTOT, MQFTOT, NQFTOT are fuselage aerodynamic loading coefficients and found by using α_{WF}, β_{WF}, Q_{WF} and fuselage aerodynamic tables as explained in reference [1].

Finally, these forces and moments in wind axis need to be transformed into body axes and forces need to be transferred to the center of gravity of helicopter.

$$\begin{bmatrix} X_{WF} \\ Y_{WF} \\ Z_{WF} \end{bmatrix} = \begin{bmatrix} \cos\alpha_{WF}\cos\beta_{WF} & \cos\alpha_{WF}\sin\beta_{WF} & -\sin\alpha_{WF} \\ \sin\beta_{WF} & -\cos\beta_{WF} & 0 \\ \sin\alpha_{WF}\cos\beta_{WF} & \sin\alpha_{WF}\sin\beta_{WF} & \cos\alpha_{WF} \end{bmatrix} \begin{bmatrix} -D_{FUS} \\ -Y_{FUS} \\ -L_{FUS} \end{bmatrix} \tag{2.23}$$

$$\begin{bmatrix} L_{WF} \\ M_{WF} \\ N_{WF} \end{bmatrix} = \begin{bmatrix} L_{WFWF} \\ M_{WFWF} \\ N_{WFWF} \end{bmatrix} + \begin{bmatrix} -Y_{WF}W_{WT} + Z_{WF}B_{WT} \\ -Z_{WF}F_{WT} + X_{WF}W_{WT} \\ +Y_{WF}F_{WT} - X_{WF}B_{WT} \end{bmatrix} \tag{2.24}$$

where

$$\begin{bmatrix} L_{WFWF} \\ M_{WFWF} \\ N_{WFWF} \end{bmatrix} = \begin{bmatrix} \cos\alpha_{WF}\cos\beta_{WF} & \cos\alpha_{WF}\sin\beta_{WF} & -\sin\alpha_{WF} \\ \sin\beta_{WF} & -\cos\beta_{WF} & 0 \\ \sin\alpha_{WF}\cos\beta_{WF} & \sin\alpha_{WF}\sin\beta_{WF} & \cos\alpha_{WF} \end{bmatrix} \begin{bmatrix} R_{FUS} \\ -M_{FUS} \\ N_{FUS} \end{bmatrix} \tag{2.25}$$

2.1.4. Empennage Model

The empennage model includes the horizontal and vertical tail model. The lift and drag forces of them are calculated using aerodynamic coefficients, velocity, density and reference area.

Horizontal tail model is based on reference [1]. Horizontal tail model mathematical formulations are given below.

Horizontal tail forces in wind axis are determined by;

$$D_{HT} = Q_{HT} * S_{HT} * C_{D_{HT}} \tag{2.26}$$

$$Y_{HT} = 0 \tag{2.27}$$

$$L_{HT} = Q_{HT} * S_{HT} * C_{L_{HT}} \tag{2.28}$$

where Q_{HT} is dynamic pressure at the horizontal tail.

Finally, these forces in wind axis need to be transformed into body axes and transferred to the center of gravity of helicopter.

$$\begin{bmatrix} X_{HT} \\ Y_{HT} \\ Z_{HT} \end{bmatrix} = \begin{bmatrix} \cos\alpha_{HT}\cos\beta_{HT} & \cos\alpha_{HT}\sin\beta_{HT} & -\sin\alpha_{HT} \\ \sin\beta_{HT} & -\cos\beta_{HT} & 0 \\ \sin\alpha_{HT}\cos\beta_{HT} & \sin\alpha_{HT}\sin\beta_{HT} & \cos\alpha_{HT} \end{bmatrix} \begin{bmatrix} -D_{HT} \\ -Y_{HT} \\ -L_{HT} \end{bmatrix} \tag{2.29}$$

$$\begin{bmatrix} L_{HT} \\ M_{HT} \\ N_{HT} \end{bmatrix} = \begin{bmatrix} Y_{HT}W_{HT} - Z_{HT}B_{HT} \\ -X_{HT}W_{HT} + Z_{HT}F_{HT} \\ -Y_{HT}F_{HT} + X_{HT}B_{HT} \end{bmatrix} \tag{2.30}$$

Vertical tail model is based on reference [1]. Vertical tail model mathematical formulations are given below.

Vertical tail forces in wind axis are determined by;

$$D_{VT} = Q_{VT} * S_{VT} * C_{D_{VT}} \tag{2.31}$$

$$Y_{VT} = Q_{VT} * S_{VT} * C_{L_{VT}} \tag{2.32}$$

$$L_{VT} = 0 \tag{2.33}$$

Finally, these forces in wind axis need to be transformed into body axes and transferred to the center of gravity of helicopter.

$$\begin{bmatrix} X_{VT} \\ Y_{VT} \\ Z_{VT} \end{bmatrix} = \begin{bmatrix} \cos\alpha_{VT}\cos\beta_{VT} & \cos\alpha_{VT}\sin\beta_{VT} & -\sin\alpha_{VT} \\ \sin\beta_{VT} & -\cos\beta_{VT} & 0 \\ \sin\alpha_{VT}\cos\beta_{VT} & \sin\alpha_{VT}\sin\beta_{VT} & \cos\alpha_{VT} \end{bmatrix} \begin{bmatrix} -D_{VT} \\ Y_{VT} \\ 0 \end{bmatrix} \tag{2.34}$$

$$\begin{bmatrix} L_{VT} \\ M_{VT} \\ N_{VT} \end{bmatrix} = \begin{bmatrix} Y_{VT}W_{VT} - Z_{VT}B_{VT} \\ Z_{VT}F_{VT} - X_{VT}W_{VT} \\ -Y_{VT}F_{VT} + X_{VT}B_{VT} \end{bmatrix} \tag{2.35}$$

2.2. Environment Model

In environment model, two subblocks of MATLAB Aerospace Blockset are used. The Input LLA contains geodetic latitude, longitude and altitude information of helicopter. The first subblock is called as “ISA Atmosphere Model”. The air temperature, air density, air speed, static pressure and dynamic pressure are calculated in this model as a function of altitude. The values given in Table 2.2 are selected for calculations of this block.

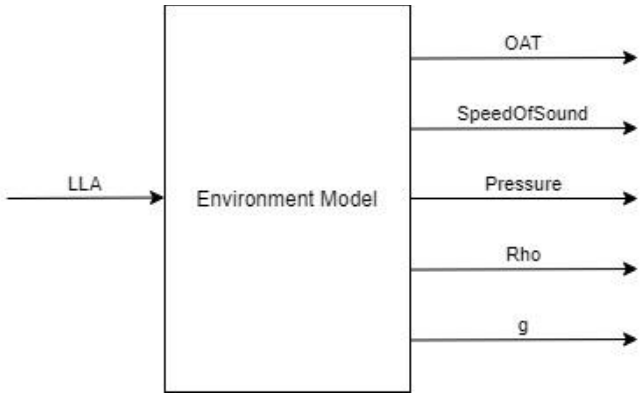

Figure 2.4. Block of environment model

The output of the environment model is defined in Table 2.3.

Table 2.2. *List of parameters for environment model*

Parameter Name	**Value**	**Unit**
Acceleration due to gravity (g)	9.80665	m/s^2
Ratio of specific heats (γ)	1.4	-
Characteristic gas constant (R)	287.0531	N*m/(kmol*K)
Laplace rate (L)	-0.0065	K/m
Height of troposphere	11000	m
Height of tropopause	20000	m
Air density at mean sea level (ρ_0)	1.225	kg/m^3
Ambient pressure at mean sea level (P_0)	101325	Pa (N/m^3)
Ambient temperature at mean sea level (T_0)	288.15	K
Lowest altitude	0	m

Table 2.3. *Description of environment model output*

Variable Name:	**Description**
OAT	Outside air temperature in degree
SpeedOfSound	Speed of sound in meter per second
Pressure	Pressure in Pascal
Rho	Density in slug feet cube
g	Gravity in feet per second square

The equations used for the calculations are listed below.

Temperature calculation,

$$T = T_0 + Lh \tag{2.36}$$

where h is altitude.

Speed of sound calculation,

$$a = \sqrt{\gamma * R * T} \tag{2.37}$$

Static pressure calculation,

$$P = P_0 * \left(\frac{T}{T_0}\right)^{\frac{g}{R*L}} \tag{2.38}$$

Air density calculation,

$$\rho = \rho_0 * \left(\frac{T}{T_0}\right)^{\frac{g}{R*L}-1} \tag{2.39}$$

The second subblock used for environment model is called as “World Geodetic System (WGS84)”. WGS84 Taylor series is selected as the type of gravity model. The position of helicopter in geodetic latitude, longitude and altitude is given as an input. The output is down gravity in North-East-Down (NED) coordinate system.

2.3. Weight and Balance Model

A script is generated for weight and balance (WAB) model. CG values and weight without fuel mass are provided by the system at initial time. The model is updated with the current fuel data when the simulation is run. The positions of helicopter parts according to helicopter cg, weight and total inertia are obtained as outputs. The total mass output of WAB model are moved to body axis with phi, theta, psi and DCM to calculate body weight.

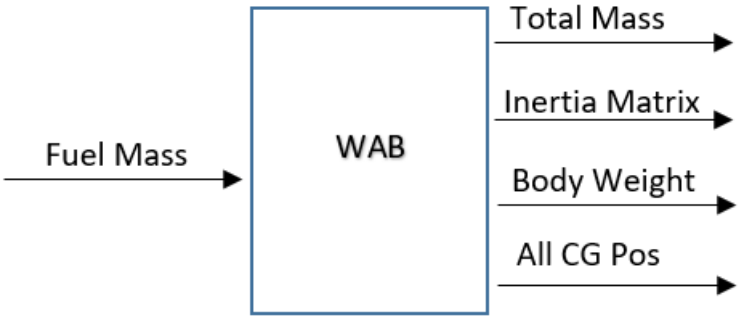

Figure 2.5. Schematic representation of WAB block

The output “All_CG_pos” includes the parameters in Table 2.4.

Table 2.4. *Description of All_CG_pos output*

Variable Name	**Description**
Pos_MR_CG	Main rotor position with respect to CG
Pos_TR_CG	Tail rotor position with respect to CG
Pos_FUS_CG	Fuselage position with respect to CG
Pos_HT_CG	Horizontal tail position with respect to CG
Pos_VT_CG	Vertical tail position with respect to CG
Pos_LG_CG	Landing gears positions with respect to CG

2.4. Equations of Motion

The present block of MATLAB named as 6DOF ECEF is used for EOM calculations. The initial values of body velocity, Euler orientation, body rotation rates and position parameters are determined to the system at the beginning. Forces, moments, body weight, total mass and total inertia values are given as inputs to the system. If required, height of train information can also be given. It is assumed as zero in this study.

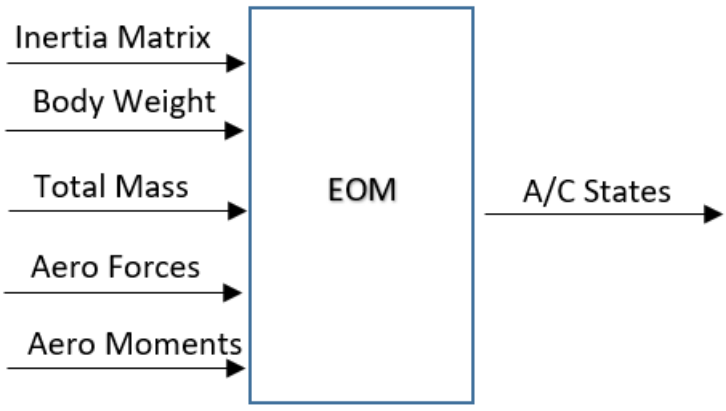

Figure 2.6. Schematic representation of EOM block

The output of EOM model is aircraft states (A/C States). The parameters of this output are listed below.

- North, East, down velocities
- Ground speed
- Vertical speed
- Attitude (phi, theta, psi)
- Altitude
- Lateral and longitudinal position
- Body velocities
- Body rotation rates
- The angular accelerations of the body
- The accelerations of the body
- The coordinate transformation from ECEF axes to NED axes

The 6DOF ECEF (Quaternion) block considers the rotation of an Earth-centered Earth-fixed (ECEF) coordinate frame ($\mathbf{X_{ECEF}}$, $\mathbf{Y_{ECEF}}$, $\mathbf{Z_{ECEF}}$) about an Earth-centered inertial (ECI) reference frame ($\mathbf{X_{ECI}}$, $\mathbf{Y_{ECI}}$, $\mathbf{Z_{ECI}}$). The origin of the ECEF coordinate frame is the center of the Earth.

The translational motion of the ECEF coordinate frame is given below, where the applied forces $[\mathbf{F_x}\ \mathbf{F_y}\ \mathbf{F_z}]^T$ are in the body frame.

$$\bar{F}_b = \begin{bmatrix} F_x \\ F_y \\ F_z \end{bmatrix} = m\left(\dot{\bar{V}_b} + \bar{w}_b \times \bar{V}_b + DCM_{bf}\bar{w}_e \times \bar{V}_b + DCM_{bf}\left(\bar{w}_e \times \left(\bar{w}_e \times \bar{X}_f\right)\right)\right) \quad (2.40)$$

where the change of position in ECEF $\bar{X}_f$ is calculated by

$$\bar{X}_f = DCM_{fb}\bar{V}_b \quad (2.41)$$

The velocity of the body with respect to ECEF frame, expressed in body frame (V_b), angular rates of the body with respect to ECI frame, expressed in body frame (w_b). Earth rotation rate (w_e), and relative angular rates of the body with respect to NED frame, expressed in body frame (w_{rel}) are defined as

$$\bar{V}_b = \begin{bmatrix} u \\ v \\ w \end{bmatrix} \tag{2.42}$$

$$\bar{w}_{rel} = \begin{bmatrix} p \\ q \\ r \end{bmatrix} \tag{2.43}$$

$$\bar{w}_e = \begin{bmatrix} 0 \\ 0 \\ w_e \end{bmatrix} \tag{2.44}$$

$$\bar{w}_b = \bar{w}_{rel} + DCM_{bf}\bar{w}_e + DCM_{be}\bar{w}_{ned} \tag{2.45}$$

$$\bar{w}_{ned} = \begin{bmatrix} V_e/(N+h) \\ -V_N/(M+h) \\ V_e \cdot \tan\mu/(N+h) \end{bmatrix} \tag{2.46}$$

The rotational dynamics of the body defined in body-fixed frame are given below,

$$A_{bb} = \begin{bmatrix} \dot{u}_b \\ \dot{v}_b \\ \dot{w}_b \end{bmatrix} = \frac{1}{m}\bar{F}_b - \left(\bar{w}_b \times \bar{V}_b + DCM_{bf}\,\bar{w}_e \times \bar{V}_b + DCM_{bf}\left(\bar{w}_e \times (\bar{w}_e \times \bar{X}_f)\right)\right) \tag{2.47}$$

$$\bar{M}_b = \begin{bmatrix} L \\ M \\ N \end{bmatrix} = I\dot{\bar{w}}_b + \bar{w}_b \times (I\bar{w}_b) \tag{2.48}$$

$$I = \begin{bmatrix} I_{xx} & -I_{xy} & -I_{xz} \\ -I_{yx} & I_{yy} & -I_{yz} \\ -I_{zx} & -I_{zy} & I_{zz} \end{bmatrix} \tag{2.49}$$

The integration of the rate of change of the quaternion vector is given below.

$$\begin{bmatrix}\dot{q}_0\\ \dot{q}_1\\ \dot{q}_2\\ \dot{q}_3\end{bmatrix} = -1/2\begin{bmatrix}0 & w_b(1) & w_b(2) & w_b(3)\\ -w_b(1) & 0 & -w_b(3) & w_b(2)\\ -w_b(2) & w_b(3) & 0 & -w_b(1)\\ -w_b(3) & -w_b(2) & w_b(1) & 0\end{bmatrix}\begin{bmatrix}q_0\\ q_1\\ q_2\\ q_3\end{bmatrix} \quad (2.50)$$

2.5. Automatic Flight Control System

AFCS has two steps. The first one is the logic step. It determines the modes to be active/passive and also which autopilot mode will be active on which control channel are decided in this step.

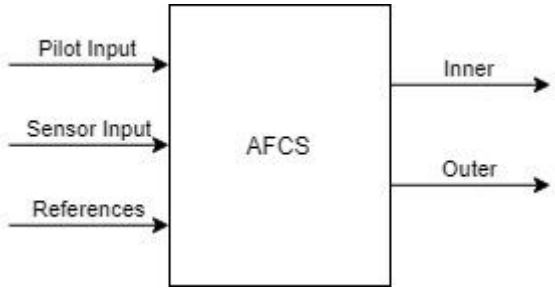

Figure 2.7. Schematic representation of AFCS block

The AFCS has several inputs. The sensor input includes indicated air speed (IAS) and weight on wheel (WOW) data. The second input is pilot input. The contents of pilot input given in Table 2.5. The autopilot has the following modes, Attitude hold (ATT), Heading hold (HDG), IAS hold, Altitude hold (ALT) and Hover (HVR) modes. The modes of autopilot can be started as open at beginning of simulation. The open/close conditions of the modes can be also selected during simulation.

Table 2.5. *Description of pilot input*

Input Name:	**Description**
AutoPilotEngaged	On/Off state of Auto pilot
ATT_Requested	On/Off state of ATT mode
IAS_Requested	On/Off state of IAS mode
ALT_Requested	On/Off state of ALT mode
HDG_Requested	On/Off state of HDG mode
HVR_Requested	On/Off state of HVR mode

The output of AFCS block is shown in Table 2.6. In AFCS block, inputs for collective, cyclic and pedal depending on active autopilot modes and their reference values are generated. AFCS is designed using classical control theory. Sequential loop closing method is used. In this method an inner loop linear control model is designed for SAS to ease the pilot's control. After the implementation of the inner loop controllers, outer loop controllers is designed. These outer loop modes are usually called flight directory modes or upper automatic flight control system modes of the helicopter.

Table 2.6. *Description of AFCS output*

Output Name:	**Description**
Inner	Pitch, Roll and Yaw commands of inner loop
Outer	Collective, Lateral cyclic, Longitudinal cyclic and Pedal commands of outer loop

In addition, reference values can be changed during flight. The changeable reference values are shown in Table 2.7. If no specific reference is entered, the related mode uses value as a reference when the mode is activated.

Table 2.7. *Description of reference input*

Reference Name:	Description
IAS_Ref	Reference value of IAS
ALT_Ref	Reference value of ALT
HDG_Ref	Reference value of HDG
Theta_Ref	Reference value of theta
Psi_Ref	Reference value of psi
Phi_Ref	Reference value of phi

Three different SAS are designed for pitch, roll and yaw axis. The inner loop control model is usually achieved by feeding back body angular rates. Pitch angular rate feedback is used in the longitudinal part where roll and yaw angular rate feedbacks are used in the lateral part. Inputs of SAS blocks are active/passive conditions of SAS mode, body angular velocities and IAS. The coefficients are defined with IAS. The outputs of SAS blocks are not sent to collective, cyclic or pedal. They effect directly to the blades and have authority of 20% of all movement field. The example for SAS blocks is given Figure 2.8. As an example, SAS model belonging to roll channel is given.

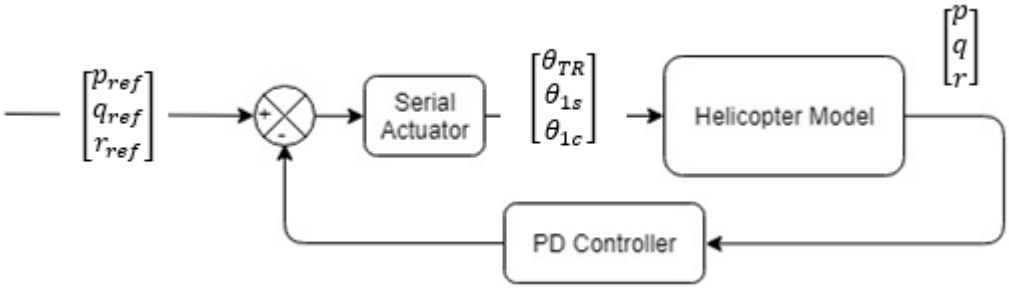

Figure 2.8. Diagram of SAS

ATT hold mode is a necessary mode for the realization of other flight directory modes such as altitude hold. If it is left uncontrolled, this can cause instability. ATT mode is designed in three axes as similar to SAS mode. The controller block for pitch channel is given in the Figure 2.9. In addition to PID controller, another parameter is added depending on the reference value. The reactions are accelerated by this feed forward controller. If ATT mode is inactive in pitch channel, both integrator and output of the model are zeroized.

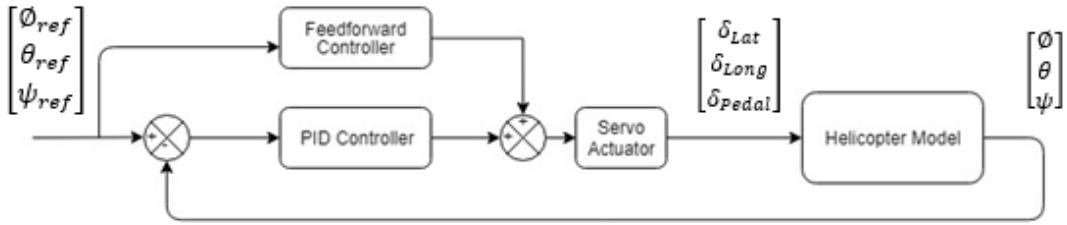

Figure 2.9. Diagram of ATT

Velocity hold mode is designed for forward flight condition. When the velocity hold mode is activated, body axis longitudinal velocity goes to the desired velocity and after that desired velocity is conserved. Block view of IAS mode of autopilot is given below. The speed error is found from the difference between reference and current speed. The first PID controller calculates a pitch error by using this speed error. This pitch error transforms into command in pitch axis after passing through another PID controller. By this second controller mechanism, discrepancy between ATT pitch and IAS, which are inputs to the same channel, is eliminated.

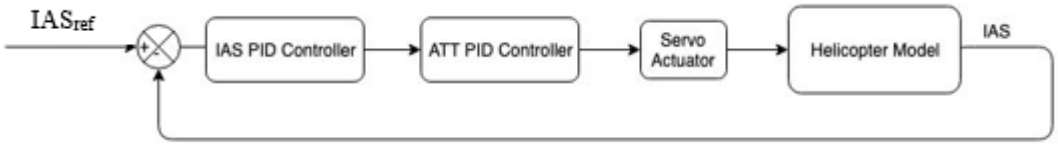

Figure 2.10. Diagram of IAS

Heading hold mode is designed to control the heading angle through pedal input. PID controller is used for HDG mode. As in the other modes, no command generation and integrator zeroizing is also available when the mode is not active.

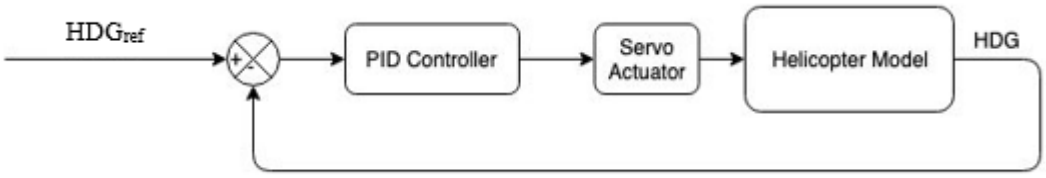

Figure 2.11. Diagram of HDG

Altitude hold mode is considered in order to design a controller to keep the helicopter at a desired altitude. The main input for controlling altitude is the collective control input. Altitude mode is controlled by PID controller and by a parameter which depend on the vertical speed (VS).

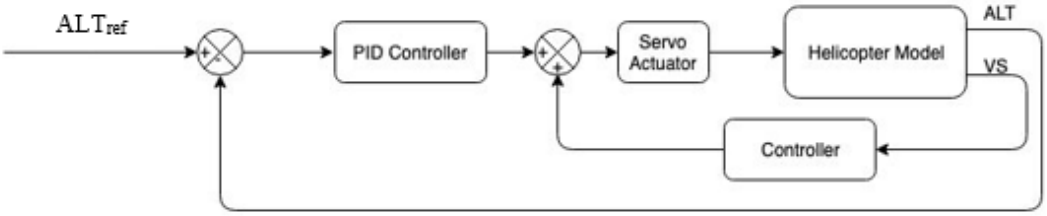

Figure 2.12. Diagram of ALT

HVR mode intends to hold longitudinal and latitudinal speeds as zero. It has two different PID controller for two different speeds. When HVR mode is activated, ALT mode holds altitude and HDG mode holds heading angle.

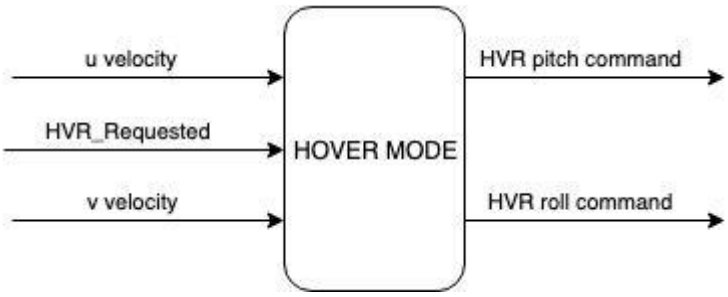

Figure 2.13. Diagram of HVR

"u" and "v" velocities are expressed in body axis. As an example, the diagram of the model which zeroizes the u velocity is given below.

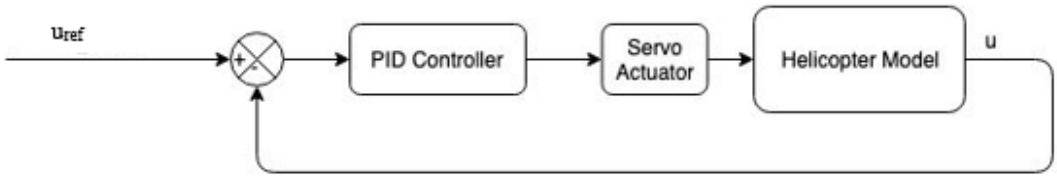

Figure 2.14. Diagram of HVR

2.6. Flight Control System

This block gets the outputs of autopilot model to calculate the angles of main rotor and tail rotor blades. The output of AFCS block (Inner and Outer) are used as input and pilot inputs (cyclic, collective and pedal) are added them. Collective pitch angle (θ_0), Longitudinal cyclic pitch (θ_{1S}), Lateral cyclic pitch (θ_{1C}) and tail rotor pitch angle (θ_{TR}) are calculated as output. Reference [1] is used as the source.

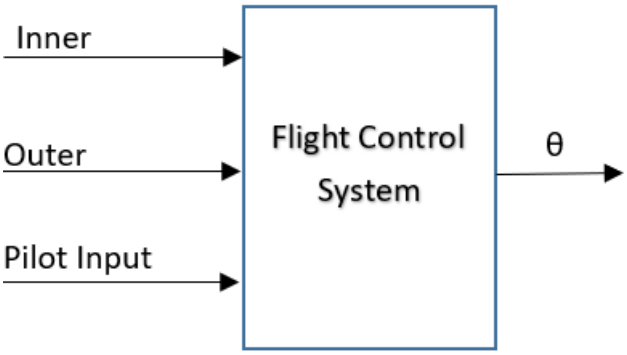

Figure 2.15. Schematic representation of FCS block

CHAPTER 3

TRIM ALGORITHM DEVELOPMENT

Trim of a helicopter is the situation in which all the forces, including aerodynamic, inertial and gravitational, as well as total moment vectors are in balance in the three mutually perpendicular axes without any further control input. In this Chapter the trim algorithms are described that are developed for the helicopter model described in Chapter 2.

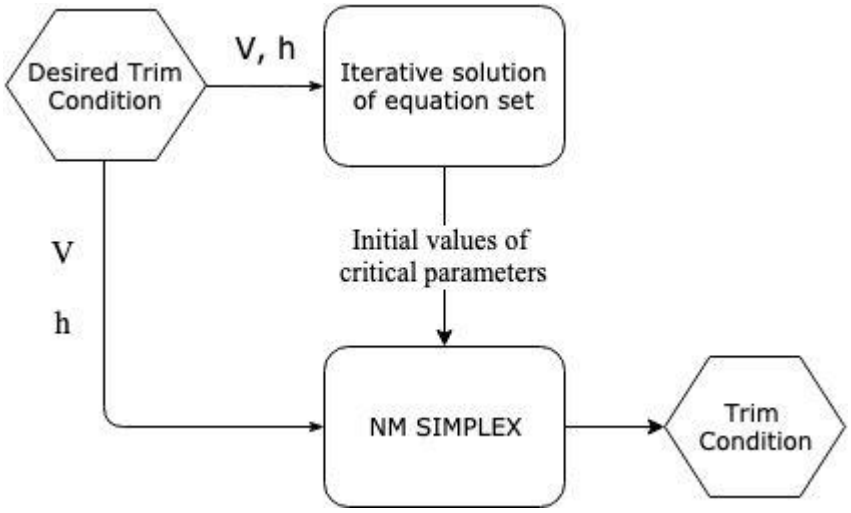

Figure 3.1. Flow chart of the trim algorithm.

Figure 3.1 shows the flow chart of the trim algorithm. To start with a set of simulations is run in order to determine the critical parameters. The criticality of a specific parameter is decided by setting this parameter to zero at the initial condition of the system runs while all the other parameters are fixed at their original values found with AFCS. The critical parameters are determined by comparing their impact on the time

to reach the trim condition. The equation set is decided and solved iteratively. The formalism and the assumptions for obtaining the equations are described in references [30] and [31]. The method to solve this equation set are detailed and the implementation of them in the trim algorithms developed are discussed. Finally, NM simplex method is described and the parameters of cost function are given.

Trim is summarized in Section 3.1. In Section 3.2 critical parameters for trim are pointed out. In the final section of Chapter 3, the algorithms used are detailed and the goals for the algorithm development are defined.

3.1. Trim Definition

Total forces on the body frame shown in equation (3.1) is the sum of the aerodynamic forces obtained from vertical tail (eqn. 2.78), horizontal tail (eqn. 2.95), fuselage (eqn. 2.60), tail rotor (eqn. 2.18), main rotor (eqns. 2.39-2.41) and gravitational force (X_{Weight}). Besides total moments on the body frame shown in equation (3.2) is the sum of the aerodynamic moments obtained from vertical tail (eqn. 2.96), horizontal tail (eqn. 2.79), fuselage (eqn. 2.61), tail rotor (eqn. 2.19) and main rotor (eqns. 2.42-2.44). In the trim condition, the total forces and the moments acting on helicopter equal to zero. When all forces and moments about three mutually perpendicular axes are equal, the aircraft is in a state of equilibrium. That equilibrium state is called as trim.

When considering the flapping and feathering of the blades of both main rotor and the tail rotor, the motion of the main rotor with respect to the fuselage, the swash plate mechanism, and the moving horizontal stabilizer in some of the helicopters, there are many equations of motion that one should solve for analysis.

$$\sum \vec{F} = 0$$

where $\vec{F} = [F_X \;\; F_Y \;\; F_Z]^T$

$$F_X = X_{V1} + X_{H1} + X_{WF} + X_{TR} + X_{MR} + X_{Weight}$$

$$F_Y = Y_{V1} + Y_{H1} + Y_{WF} + Y_{TR} + Y_{MR} + Y_{Weight} \quad \textbf{(3.1)}$$

$$F_Z = Z_{V1} + Z_{H1} + Z_{WF} + Z_{TR} + Z_{MR} + Z_{Weight}$$

$$\sum \vec{M} = 0$$

where $\vec{M} = [M_X \;\; M_Y \;\; M_Z]^T$

$$M_X = L_{V1} + L_{H1} + L_{WF} + L_{TR} + L_{MR}$$

$$M_Y = M_{V1} + M_{H1} + M_{WF} + M_{TR} + M_{MR} \quad \textbf{(3.2)}$$

$$M_Z = N_{V1} + N_{H1} + N_{WF} + N_{TR} + N_{MR}$$

Because of the fact that a helicopter has so many degrees of freedom, it is much more difficult to analyze its equilibrium compared to a fixed-wing aircraft which can generally be modelled as a rigid body with 6 degrees of freedom (DOF). For the helicopter the fuselage has 6 DOFs, the main rotor has 4 DOFs (3 for rotor flapping and one for the rotation of the rotor (throttle)), tail rotor has also 4 DOFs, etc. However, with some feasible assumptions, the helicopter system can be reduced to 6 DOF like a fixed-wing aircraft, three for translation and three for rotation.

A helicopter with a main rotor and a tail rotor, assuming it as having a rigid structure, has more than 20 non-linear equations, which makes the problem very difficult to solve. The following general simplifications are implemented in order to simplify the set of equilibrium equations for trim analysis:

– The helicopter structure is considered to be absolutely rigid;

– The blades are assumed as uniform and the lag bending, elastic twist, and axial deflections are disregarded, except the flapping motion;

– The blades have homogeneous mass distribution;

On the basis of these assumptions, the equations of motion given in Chapter 2 can be simplified furthermore.

3.2. Parameter Selection

General view of helicopter dynamics is shown in equation 3.3

$$\dot{x} = f(x,t,u) \tag{3.3}$$

Input vector is given in equation 3.4 and sate vector is given in equation 3.5.

$$u = [\delta_{Lat} \quad \delta_{Long} \quad \delta_{Pedal} \quad \delta_{Coll}] \tag{3.4}$$

$$x = [u \quad v \quad w \quad p \quad q \quad r \quad \emptyset \quad \theta \quad \psi] \tag{3.5}$$

Input vector is also written in terms of blade angles as given equation 3.6.

$$u = [\theta_{1C} \quad \theta_{1S} \quad \theta_{TR} \quad \theta_0] \tag{3.6}$$

It is necessary to trim main and tail rotor systems for the integrity of trim condition. The new state vector is given in equation 3.7. It is obtained by adding altitude, main rotor and tail rotor parameters to the state vector given in equation 3.5.

$$x = \begin{bmatrix} u & v & w & p & q & r & \emptyset & \theta & \psi & \vec{\lambda}_{MR} & \lambda_{TR} & \vec{\beta} & \dot{\vec{\beta}} & h \end{bmatrix} \quad \textbf{(3.7)}$$

Inflow model has three states. They are given in equation 3.8. The uniform flow (λ_0) is related to thrust coefficient. The linearly varying lateral and longitudinal (λ_{1S} and λ_{1C}) inflow states are related to rolling and pitching moments generated by main rotor.

$$\vec{\lambda}_{MR} = [\lambda_0 \ \lambda_{1S} \ \lambda_{1C} \ ]^T \quad \textbf{(3.8)}$$

The formulization of $\vec{\lambda}_{MR}$ [32] at the disc are given eqn 3.9

$$\lambda = \lambda_0 + \lambda_{1S} \, r \sin\psi + \lambda_{1C} \, r \cos\psi \quad \textbf{(3.9)}$$

where r is radial distance.

β and $\dot{\beta}$ given by equations 3.10 and 3.11 are considered explicitly for each blade mentioned in Chapter 2.1.1.

$$\vec{\beta} = [\beta_1 \ \beta_2 \ \beta_3 \ \beta_4 \ \beta_5 \ \beta_6 \ \beta_7 \ \beta_8 \ \beta_9 \ \beta_{10} \ \beta_{11} \ \beta_{12}]^T \quad \textbf{(3.10)}$$

$$\dot{\vec{\beta}} = [\dot{\beta}_1 \ \dot{\beta}_2 \ \dot{\beta}_3 \ \dot{\beta}_4 \ \dot{\beta}_5 \ \dot{\beta}_6 \ \dot{\beta}_7 \ \dot{\beta}_8 \ \dot{\beta}_9 \ \dot{\beta}_{10} \ \dot{\beta}_{11} \ \dot{\beta}_{12}]^T \quad \textbf{(3.11)}$$

Instead of calculating β for each blade, the equations 3.12-3.14 of β_0, β_{1S} and β_{1C} can be used.

$$\beta_0 = \frac{1}{NBS}\sum_{m=1}^{NBS}\beta_m \quad \textbf{(3.12)}$$

$$\beta_{1C} = \frac{2}{NBS}\sum_{m=1}^{NBS}\beta_m \cos\varphi_m \quad \textbf{(3.13)}$$

$$\beta_{1S} = \frac{2}{NBS}\sum_{m=1}^{NBS}\beta_m \sin\varphi_m \quad \textbf{(3.14)}$$

where NBS is total blade number.

Similarly, instead of calculating $\dot{\beta}$ for each blade, the equations 3.15-3.17 of $\dot{\beta}_0$, $\dot{\beta}_{1S}$ and $\dot{\beta}_{1C}$ can be used.

$$\dot{\beta}_0 = \frac{1}{NBS}\sum_{m=1}^{NBS}\dot{\beta}_m \quad \textbf{(3.15)}$$

$$\dot{\beta}_{1C} = \frac{2}{NBS}\sum_{m=1}^{NBS}(\dot{\beta}_m \cos\psi_m - \beta_m \Omega \sin\psi_m) \quad \textbf{(3.16)}$$

$$\dot{\beta}_{1S} = \frac{2}{NBS}\sum_{m=1}^{NBS}(\dot{\beta}_m \sin\psi_m + \beta_m \Omega \cos\psi_m) \quad \textbf{(3.17)}$$

The desired value of trim parameters for hover and forward flight are given equations 3.18-3.21.

$$p = q = r = \psi = \dot{\beta}_0 = \dot{\beta}_{1S} = \dot{\beta}_{1C} = 0 \quad \textbf{(3.18)}$$

$$h = h_{reference} \quad \textbf{(3.19)}$$

$$u = u_{reference} \tag{3.20}$$

$$v = v_{reference} \tag{3.21}$$

The constraints of helicopter parameters for trim are given equation 3.22-3.25.

$$\dot{u} = \dot{v} = \dot{w} = 0 \tag{3.22}$$

$$\dot{p} = \dot{q} = \dot{r} = 0 \tag{3.23}$$

$$\ddot{\beta}_0 = \ddot{\beta}_{1S} = \ddot{\beta}_{1C} = \dot{\vec{\lambda}}_{MR} = \dot{\lambda}_{TR} = 0 \tag{3.24}$$

$$\dot{h} = 0 \tag{3.25}$$

The final set of unknown parameters, which is obtained by evaluating input vector (eqn. 3.6), state vector (eqn. 3.7), desired conditions (eqns. 3.18-3.21) and constraints (eqns. 3.22-3.25), is given in equation 3.26.

$$x = \begin{bmatrix} w & \emptyset & \theta & \beta_0 & \beta_{1S} & \beta_{1C} & \vec{\lambda}_{MR} & \lambda_{TR} & \theta_{1C} & \theta_{1S} & \theta_{TR} & \theta_0 \end{bmatrix} \tag{3.26}$$

Before starting trim algorithm development studies, various analyses are performed on dynamic main rotor parameters ($\phi, \Theta, \lambda, \Theta_0, \Theta_{1s}, \Theta_{1c}, \ddot{\beta}$, $\dot{\beta}$ and β) and tail rotor parameters ($\lambda_{TR}, \Theta_{TR}$). These parameters are defined in the list of symbols. They are investigated to determine which parameters are more effective on elapsed time for trim (ETT). For this purpose, a reference autopilot trim point (AP trim point in Figure 3.3-8) is obtained with the help of AFCS. Firstly, initial value for $\ddot{\beta}$ is equalized to zero and then simulation is run again in order to reach trim condition. For the second condition $\ddot{\beta}$ and $\dot{\beta}$ are set to zero at the same time as initial values. Similarly, β is additionally set as zero for next instance. As a final condition, just λ_{TR} is equalized to

zero. All results are presented in Figures 3.2 and 3.3. $\ddot{\beta}$ and $\dot{\beta}$ do not have significant effect on ETT. However, λ_{TR} and β have a drastic impact on ETT.

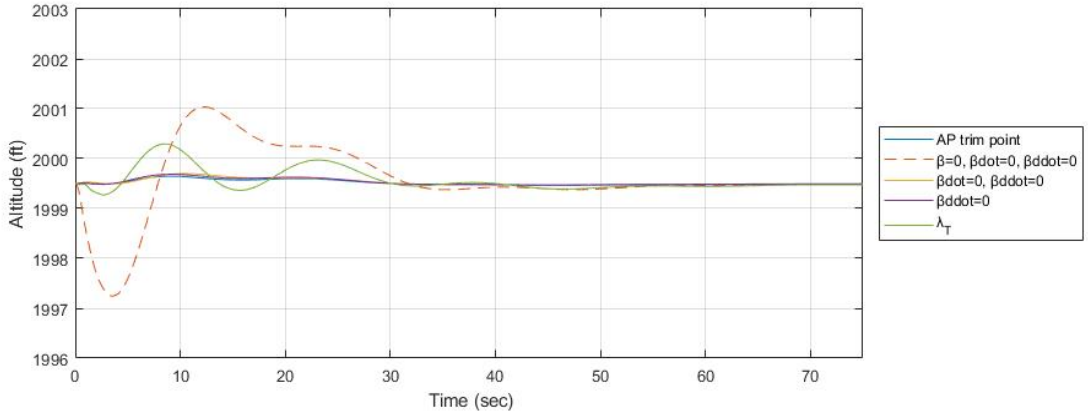

Figure 3.2. Altitude vs Time for flap parameters

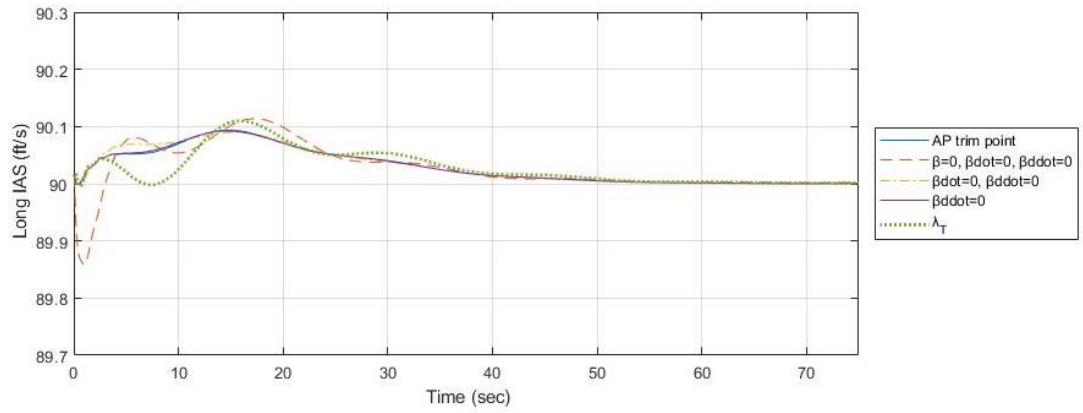

Figure 3.3. IAS vs Time for flap parameters

In the second phase of the study, simulation is run for each control channel. The positions of control channels have an important role on obtaining trim point. Reference trim point value is increased individually by 10%. Collective, lateral cyclic, longitudinal cyclic and pedal test results are presented in Figures 3.4 and 3.5

respectively. All control channels have considerable effect on ETT and it is observed that the most influential parameter is longitudinal cyclic input for IAS. It extends ETT approximately 30 seconds. Also, collective input is the most influential parameter for ALT.

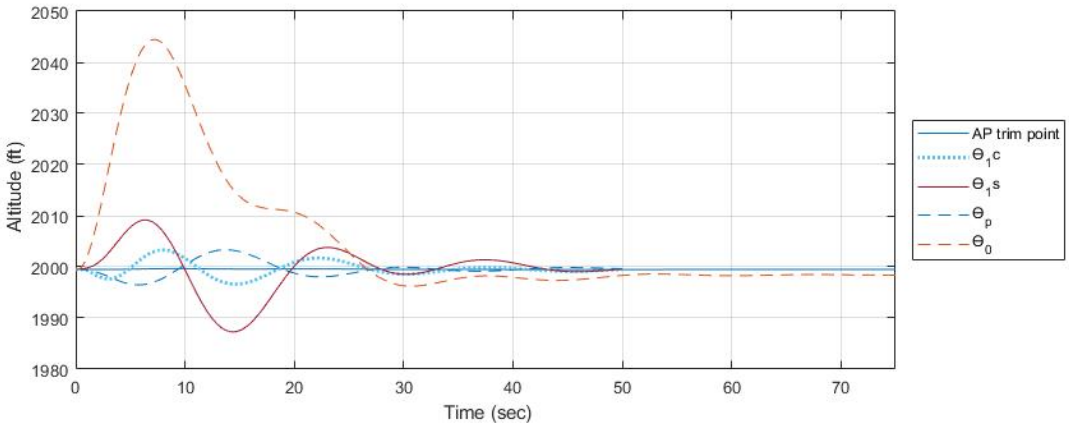

Figure 3.4. Altitude vs Time for control channel parameters

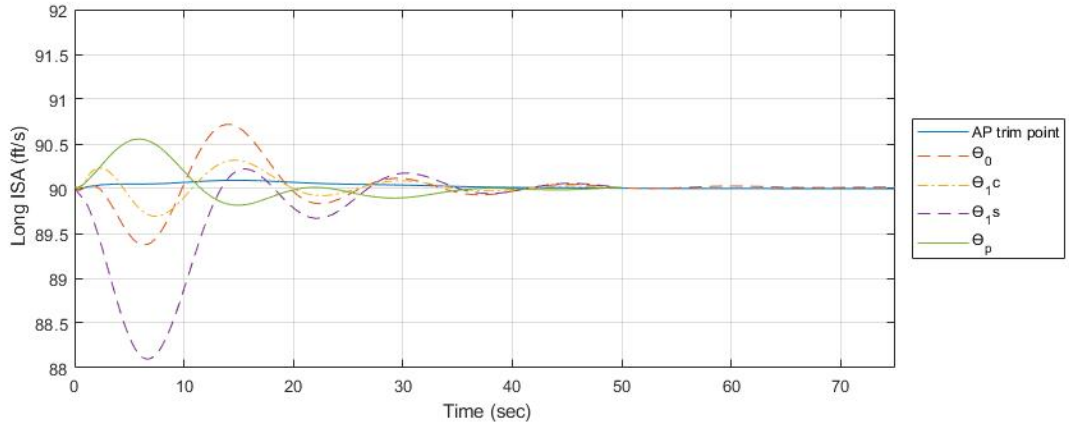

Figure 3.5. IAS vs Time for control channel parameters

For final step similar effort is performed for attitude angles. Initial values for λ, φ and θ are set to zero. As presented in Figures 3.6 and 3.7, all parameters have about two times longer ETT as compared to the AP trim point.

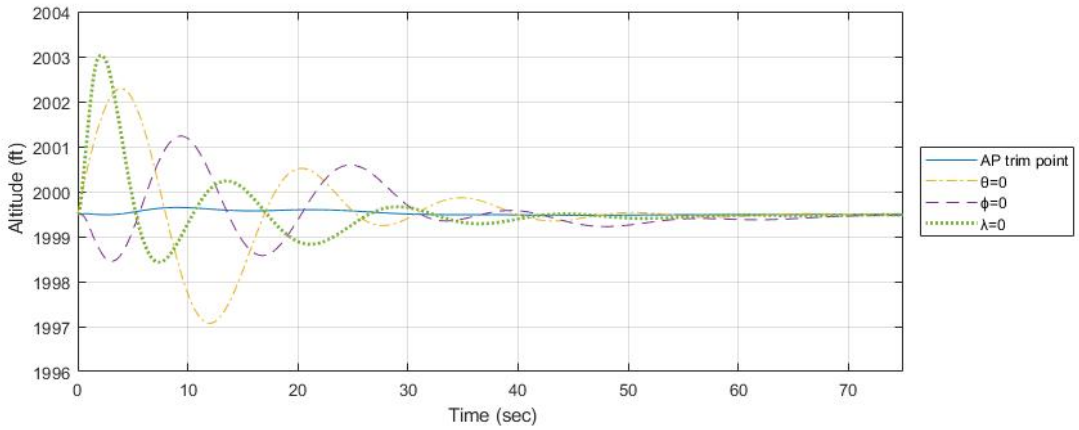

Figure 3.6. Altitude vs Time for attitude parameters

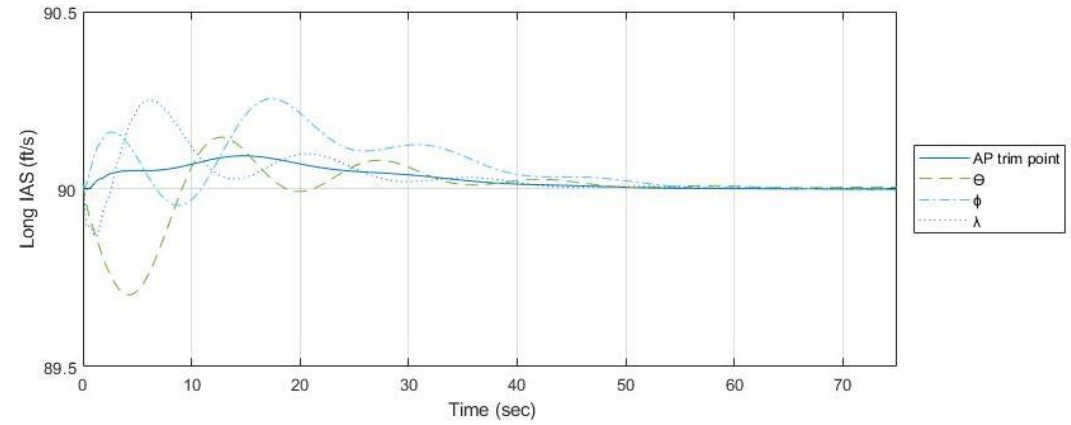

Figure 3.7. IAS vs Time for attitude parameters

Figures 3.2-3.7 show that ETT is increased two or three times for different conditions. When the default values are given at the same time for cited dynamic main rotor

parameters, unacceptable ETT extension is occurred and also for same cases trim point cannot be reached. At the end of this study critical nine parameters ($\phi, \theta, \lambda, \theta_0, \theta_{1s}, \theta_{1c}, \theta_{TR}, \lambda_{TR}, \beta$) are determined. Eventually at least eleven equations are needed to calculate them.

For the helicopter model, an equation set can be obtained by assuming that the total forces and momentum are equal to zero for trim situation. By using this equation set, better initial values can be got for these 11 parameters. The trim values of angular velocities (p, q and r) are equal to zero. Yaw angle is assumed a constant number because it has no effect on trimmed flight. Initial values of derivative and double derivative flaps parameters are taken zero due to negligible effects on ETT as shown in Figures 3.2 and 3.3. The vector of trim unknowns for rotors is:

$$\vec{X} = [\phi \ \theta \ \lambda \ \theta_0 \ \theta_{1s} \ \theta_{1c} \ \theta_{TR} \ \lambda_{TR} \ \beta_0 \ \beta_{1S} \ \beta_{1C}] \quad \textbf{(3.27)}$$

The equation set and the assumptions, that are used to find 11 unknown parameters, are explained in the next section.

3.3. Algorithm Development

In this study, two different methods are used jointly. The first method Fixed Point Iteration is described in Chapter 3.3.1 with the equations used. The results obtained from iterations are used as input for the second method, i.e. NM Simplex Method, which is detailed in Chapter 3.3.2.

3.3.1. Trim Solution Using Approximate Equations

Fixed-point iteration method is used for iterative solution Ref [29]. Method is numerically confirmed for the parameters of Y vector, as shown in Table 4.1. Y vector

is given in equation 3.28. The results obtained by applying the Fixed-Point Iteration method with the boundary values of Table 4.1 are given in Appendix B.

$$\vec{Y} = [\lambda \quad \beta_{1S} \quad \beta_{1C} \quad \alpha_S \quad \theta_{1S}\,] \tag{3.28}$$

The iteration starts to run by providing initial values to the parameters of the Y vector. If a good guess for the solution is not available, Y can be chosen randomly. Equations 3.32-3.50 are solved iteratively. The procedure is repeated until the value of cost function equation 3.51 is less than the tolerance value, which is set to 0.001.

The assumptions made and the equations used in this thesis are detailed in Ref. [30], [31] and are represented hereafter. The parameters in the equations are given in the Figures 3.8 and 3.9.

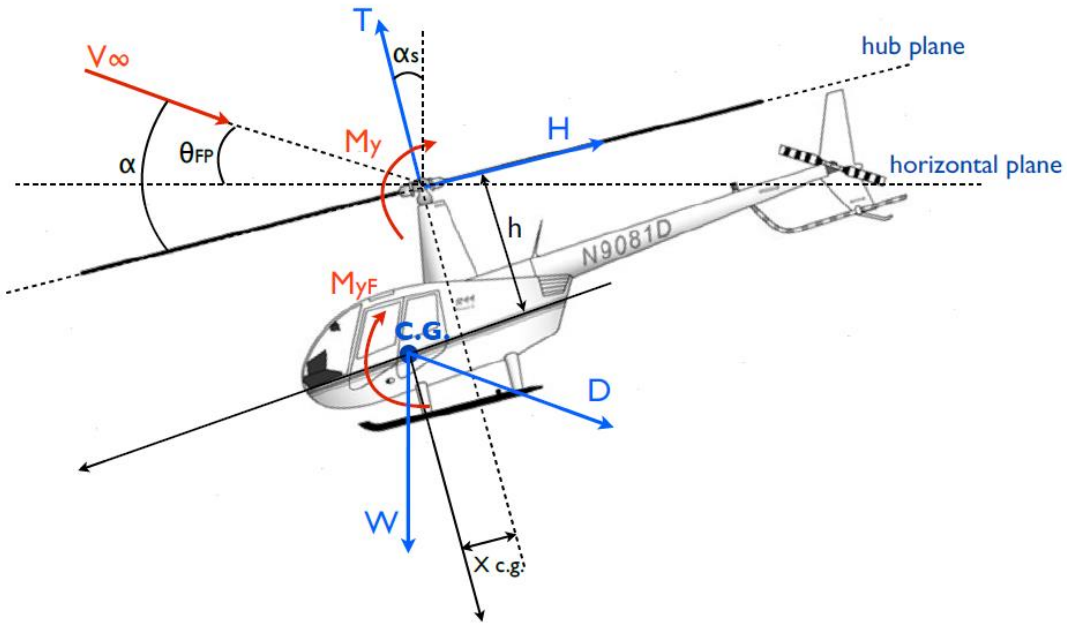

Figure 3.8. Longitudinal Forces and Moments [31]

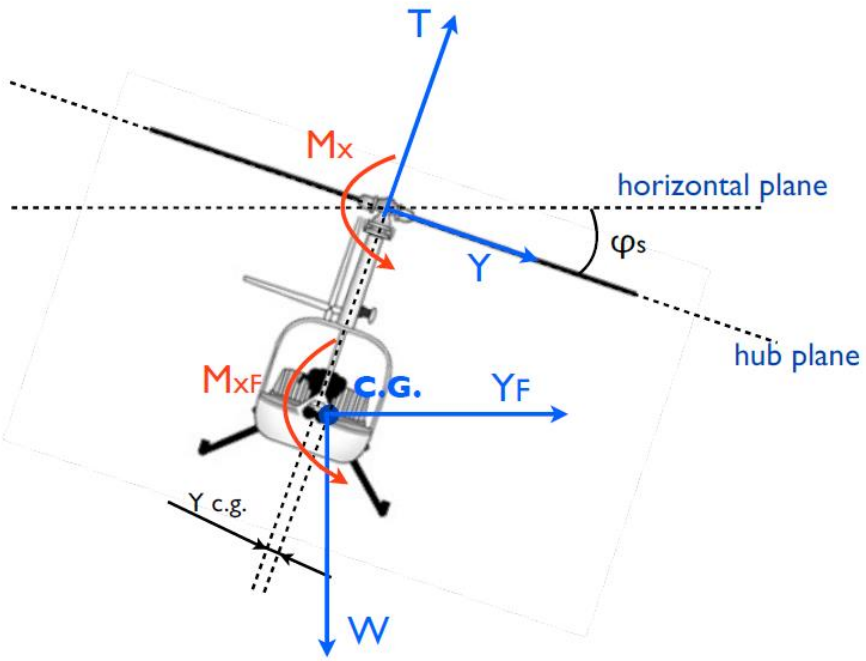

Figure 3.9. Lateral Forces and Moments [31]

Before starting of the derived trim equations, assumptions are given below.

- Rigid blades
- Uniform inflow
- No reverse flow
- No compressibility effects
- Constant drag coefficient of mean value C_{D_0}
- Tip loss and root cut out effects are neglected
- For level flight $\theta_{FP} = 0$
- Small angle assumption is made
- Actual forces and Tip path plane (TPP) forces assumed to be equal
- Constant-chord blade
- No sideslip.

The calculations are started with predicted values. Therefore, iterations must be performed. It starts with an initial guess.

$$C_T = C_W \tag{3.29}$$

For the first step all angle parameters in equation 3.30 are equal to zero. λ and λ_{TR} are equal and the value is considered as one for the first iteration. These assumptions are given in equation 3.31.

$$\theta_{1S} = \beta_{1S} = \beta_{1C} = \alpha_S = 0 \tag{3.30}$$

$$\lambda = \lambda_{TR} = 1 \tag{3.31}$$

Equations 3.32-3.50 are obtained from force and moment equilibrium. From this point on they are referred as Simplified Trim Equations (STE).

Inflow ratio:

$$\lambda = \mu\tan\alpha + \frac{C_T}{2\sqrt{\mu^2 + \lambda^2}} \tag{3.32}$$

In order to calculate an accurate inflow value, equation (3.31) is reiterated within itself with a nonzero initial value of inflow ratio.

Collective:

$$\theta_0 = \frac{3\left[\frac{2C_T}{\sigma a} - \frac{\theta_T}{4}(1+\mu^2) + \frac{\mu}{2}\theta_{1S} + \frac{\lambda}{2}\right]}{1 + \frac{3}{2}\lambda^2} \tag{3.33}$$

Cone angle:

$$\beta_0 = \frac{\vartheta_0^2}{\vartheta^2}\beta_p + \frac{\gamma}{\vartheta^2}\left[\frac{\theta_0}{8}(1+\mu^2) + \frac{\theta_T}{10}\left(1+\frac{5}{6}\mu^2\right) - \frac{\mu}{6}\theta_{1S} - \frac{\lambda}{6}\right] \quad (3.34)$$

Lateral cyclic:

$$\theta_{1C} = \beta_{1S} - \frac{\frac{4}{3}\mu\beta_0 - \frac{(\vartheta^2-1)8}{\gamma}\beta_{1C}}{1+\frac{1}{2}\mu^2} \quad (3.35)$$

Longitudinal cyclic:

$$\theta_{1S} = \frac{\frac{8}{3}\mu\left(\theta_0 + \frac{3}{4}\theta_t - \frac{3}{4}\lambda_{TPP}\right) + \frac{(\vartheta^2-1)8}{\gamma}\beta_{1C}}{1+\frac{3}{2}\mu^2} - \beta_{1C} \quad (3.36)$$

Longitudinal force:

$$C_{HTPP} = \frac{\sigma C_{d0}}{4}\mu + \frac{\sigma a}{2}\left[\frac{\mu\lambda_{TPP}}{2}\left(\theta_0 + \frac{1}{2}\theta_t\right) + \frac{1}{6}\theta_{1C}\beta_0 - \frac{1}{4}\theta_{1S}\lambda_{TPP} + \frac{1}{4}\mu\beta_0^2\right] \quad (3.37)$$

Lateral force:

$$C_{YTPP} = -\frac{\sigma a}{2}\left[\frac{3}{4}\mu\beta_0\left(\theta_0 + \frac{2}{3}\theta_t\right) - \frac{1}{6}\theta_{1S}\beta_0(1+3\mu^2) - \frac{1}{4}\theta_{1C}\lambda_{TPP} - \frac{3}{2}\mu\beta_{0\lambda_{TPI}}\right. \quad (3.38)$$

Longitudinal cone angle:

$$\beta_{1C} = \frac{\frac{X_{cg}}{h} - \frac{M_{YF}}{Wh} - \frac{C_{HTPP}}{C_T}}{1 + \frac{\frac{(\vartheta^2-1)}{\gamma}}{\frac{C_T}{\sigma a}\frac{2h}{R}}} \quad (3.39)$$

Lateral cone angle:

$$\beta_{1S} = \frac{\frac{-Y_{cg}}{h} + \frac{M_{XF}}{Wh} - \frac{C_{YTPP}}{C_T}}{1 + \frac{\frac{(\vartheta^2 - 1)}{\gamma}}{\frac{C_T}{\sigma a}\,{}^{2h}/_{R}}} \tag{3.40}$$

The obtained β_0, β_{1C} ve β_{1S} values are split again on the azimuth axis, which will fit into 12 equal parts. Thus, it will be convenient to model of input.

Tip path plane tilt angle:

$$\alpha_S = \frac{\frac{X_{cg}}{h} - \frac{M_{YF}}{Wh} - \frac{\frac{(\vartheta^2 - 1)}{\gamma}}{\frac{C_T}{\sigma a}\,{}^{2h}/_{R}}\frac{C_{HTPP}}{C_T}}{1 + \frac{\frac{(\vartheta^2 - 1)}{\gamma}}{\frac{C_T}{\sigma a}\,{}^{2h}/_{R}}} + \frac{D}{W} \tag{3.41}$$

Roll angle:

$$\emptyset_S = \frac{\frac{Y_{cg}}{h} - \frac{M_{XF}}{Wh} - \frac{\frac{(\vartheta^2 - 1)}{\gamma}}{\frac{C_T}{\sigma a}\,{}^{2h}/_{R}}\frac{C_{YTPP}}{C_T}}{1 + \frac{\frac{(\vartheta^2 - 1)}{\gamma}}{\frac{C_T}{\sigma a}\,{}^{2h}/_{R}}} - \frac{Y_F}{W} \tag{3.42}$$

Weight:

$$C_w = \frac{W}{\rho\pi R^2(\pi R^2)} \tag{3.43}$$

Thrust coefficient:

$$C_T = \frac{C_w}{\cos\alpha_S} + \frac{\left(\frac{1}{2}\mu^2\left(\frac{f}{A}\right)\right)}{\cos\alpha_S}\sin\theta_{FP} - C_H\tan\alpha_S \tag{3.44}$$

Power coefficient:

$$C_P = \frac{C_T^2}{2\sqrt{\mu^2+\lambda^2}} + \frac{\sigma C_{d0}}{8}(1+4.6\mu^2) + \frac{1}{2}\mu^3\left(\frac{f}{A}\right) + C_T\lambda_c \tag{3.45}$$

Torque coefficient:

$$C_Q = C_P \tag{3.46}$$

Torque:

$$\mathrm{Q} = \frac{1}{2}\rho A\,(\Omega R)^2 R C_Q \tag{3.47}$$

Tail rotor thrust coefficient:

$$C_{T_{TR}} = \frac{\mathrm{Q}/\Delta\mathrm{L}}{\rho\pi R^2(\Omega R)^2} \tag{3.48}$$

Tail rotor inflow:

$$\lambda_{TR} = \frac{C_{T_{TR}}}{2\sqrt{\mu^2+\lambda_{TR}^2}} \tag{3.49}$$

Pedal:

$$\theta_{\mathrm{TR}} = \frac{C_{T_{TR}} * \frac{2}{\sigma a} - \frac{1}{4}\,\theta_0(1+\mu^2) + \frac{1}{2}\,\lambda_{TR}}{\frac{1}{2} + \frac{3}{4}\mu^2} \tag{3.50}$$

As a result of the iteration, the closer values to trim point are obtained for $\phi, \lambda, \theta_0, \theta_{1s}, \theta_{1c}, \theta_{TR}, \lambda_{TR}$ and β parameters. By means of the results acquired from the solution of STE, NM Simplex method started to operate from a closer value to trim point. The cost function of STE is given in the following equation.

$$\text{Cost Function} = (\Delta\phi)^2 + (\Delta\lambda)^2 + (\Delta\theta_0)^2 + (\Delta\theta_{1s})^2 + (\Delta\theta_{1c})^2 + (\Delta\beta_0)^2 + (\Delta\beta_{1s})^2 + (\Delta\beta_{1c})^2 + (\Delta\theta_{TR})^2 + (\Delta\lambda_{TR})^2 \tag{3.51}$$

The notation ΔX means the difference between old value and new value of X within iteration.

3.3.2. Nelder-Mead Simplex Method

The NM Simplex Method [32] is generally used to solve parameter estimation and similar statistical problems. It can handle discontinuous functions, where function values are uncertain or subject to noise. The algorithm is an iterative process that tries to replace the worst solution with a new and better solution at each step. A chosen simplex defines the search area. A chosen cost function directs optimization to the target solution. Each vertex stands for a result from the cost function, that is a different set of parameters to be minimized. Three vertices are ordered at the start of each iteration, from best to worst. The best point is the one with the lowest value of the objective function, the worst point is defined by the highest value and the second highest value defines the lousy point. The remaining goal is then to adjust the

parameter values of the worst point so that the simplex moves towards the function minimum. The direction of travel is determined by the centroid. The centroid is the geometric center of every point except the worst point. It is calculated at each iteration by identifying the worst point, and then taking the average of the parameter values at the remaining points. Then, a minimum point is obtained for cost function on the vertices. The trim condition is defined by this minimum point. In Figure 3.10, the operations (reflect, shrink, expand, inside and outside contractions) belonging to NM Simplex method are shown. The processing of NM Simplex algorithm is explained in Figure 3.11.

For the first simplex, each non-zero optimization parameter is sequentially increased 5% and the optimization parameter equal to zero is set to 0,00025. The variation of each optimization parameter constitutes a condition. The model is run for each condition. The first simplex is generated with the results of cost function for these conditions. The new point calculation continues by getting the average of all points except the worst one.

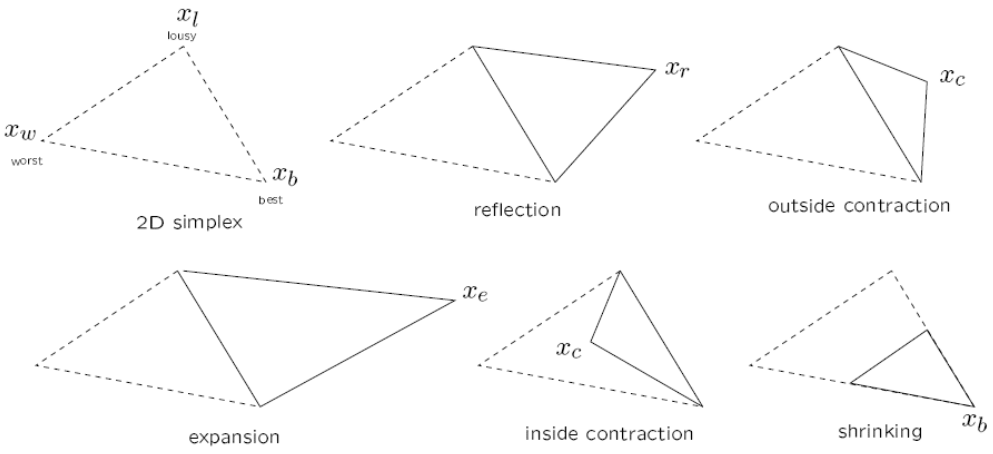

Figure 3.10. Operations performed on the simplex in Nelder-Mead's algorithm

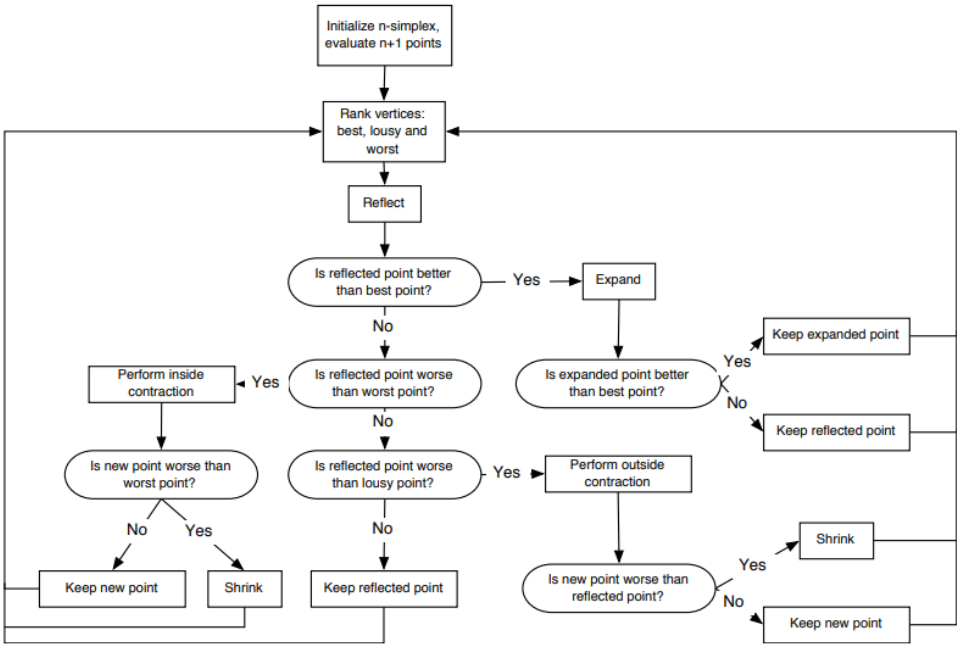

Figure 3.11. Flow chart for the Nelder-Mead algorithm

The method is quite simple and is implemented in many different ways. Two main differences between various implementations are in the construction of the initial simplex and in the selection of termination criteria. The steps of a general algorithm is given below.

- The initial working simplex S is constructed.
- The following steps are repeated until the termination criterion/test is satisfied:
  - Calculation of the termination test information;
  - If the termination test fails, transform the working simplex.
- Return the best vertex of the current simplex S and the associated function value.

In this study, NM Simplex method is executed by using "fminsearch" function of MATLAB. The cost function is given in the equation 3.52. The system is run one second (60 frames) at each trial. The cost function values at three different time frames in one second (20^{th}, 40^{th} and 60^{th} frames) are added to increase the reliability of the results.

$$\text{Cost Function} = J_{f=20} + J_{f=40} + J_{f=60} \tag{3.52}$$

where subscript f is frame number.

$$J = W\ P^T \tag{3.53}$$

$$\begin{aligned} W = [&\dot{p}_w\ \dot{q}_w\ \dot{r}_w\ \dot{u}_w\ \dot{v}_w\ \dot{w}_w\ \dot{\beta}_{0_w}\ \dot{\beta}_{1C_w}\ \dot{\beta}_{1S_w}\ \dot{\lambda}_{0_w}\ \dot{\lambda}_{1C_w}\ \dot{\lambda}_{1S_w}\ \dot{\lambda}_{TR_w} \\ &p_w\ q_w\ r_w\ h_w\ u_w\ v_w] \end{aligned} \tag{3.54}$$

$$\begin{aligned} P = [\ &\dot{p}^2\ \dot{q}^2\ \dot{r}^2\ \dot{u}^2\ \dot{v}^2\ \dot{w}^2\ \dot{\beta_o}^2\ \dot{\beta_{1C}}^2\ \dot{\beta_{1S}}^2\ \dot{\lambda_0}^2\ \dot{\lambda_{1S}}^2\ \dot{\lambda_{1C}}^2\ \dot{\lambda_{TR}}^2\ p^2\ q^2\ r^2 \\ &(h - h_{ref})^2\ (u - u_{ref})^2\ (v - v_{ref})^2] \end{aligned} \tag{3.55}$$

where W is weight vector and P vector contains the parameters of cost function.

The control parameters are four controller positions, $\emptyset, \theta$ and w values.

CHAPTER 4

RESULTS AND DISCUSSION

In this section, GENHEL results refer to the trim condition for the entire flight of the UH-60 helicopter model of reference [1]. Trim results for a specific flight in GENHEL are generated by a script developed. The purpose is to provide a comparative reference data for the UH-60 helicopter model of this thesis. In our UH-60 helicopter model main rotor/aerodynamics block is based on reference [1] and the other blocks are modeled as described in Chapter 2. AFCS refers to autopilot results for UH-60 helicopter model. AFCS results are obtained by running the entire model. The accuracy of the results obtained from AFCS are verified by operating the model both SAS ON and SAS OFF conditions. It is observed that attitude of the helicopter does not change when the system is operated on SAS ON at the trim points obtained from AFCS. Afterwards, the system is rerun with the same initial points at SAS OFF condition. It can be seen that the behavior of the model can stay stable without deterioration for a while. AFCS results are taken as the target for the trim simulations. The procedure is justified by comparing AFCS and the trim simulation result. Furthermore, the procedure is verified for the trim points that cannot be found by autopilot.

The MATLAB script written for STE includes the helicopter parameters and equations given in Section 3.2.1. It takes altitudes and velocities for the above-mentioned trim conditions. It outputs the positions of collective, cyclic and pedal, flap angles, inflow values and altitude (i.e. all the helicopter parameters given at the end of Section 3.2.). The simulation of STE has two main purposes. The first purpose is to include the dynamical model described in section 3.3.1 into simulations and to check its relevance. The second purpose is to provide initial conditions for faster and controllable

convergence of NM Simplex simulations. The script is also written for NM Simplex in MATLAB and uses "fminsearch" command of MATLAB to find the global minimum. The output parameters of iteration and the altitude and velocity information of the corresponding condition are its input set. STE code runs only one time for each trim condition and the output of the run becomes the input for the NM Simplex code. Simplex code runs the model until it finds the global minimum. For these runs h_w is taken as 10^{-6}, u_w and v_w are set to 10^{-4}, and all the other parameters are set to 1.

In this study, model is trimmed in five different conditions: hover condition at 5370 ft., 55 knot at 5020 ft., 93 knot at 6450 ft., 10 knot backward speed at 2000 ft. and 20 knot lateral speed at 2000 ft. Autopilot cannot trim the last two conditions.

The system starts with default values to find trim point by autopilot method. The desired trim point is given as the target for autopilot. For the first trim point, the model is started with autopilot at 2000 ft. hover condition, then it is raised to 5370 ft. hover condition. Speed and altitude information of the simulation can be seen in Figure 4.1. The reference values are entered to autopilot at tenth second. The expected trim point is obtained in about 3,5 minutes.

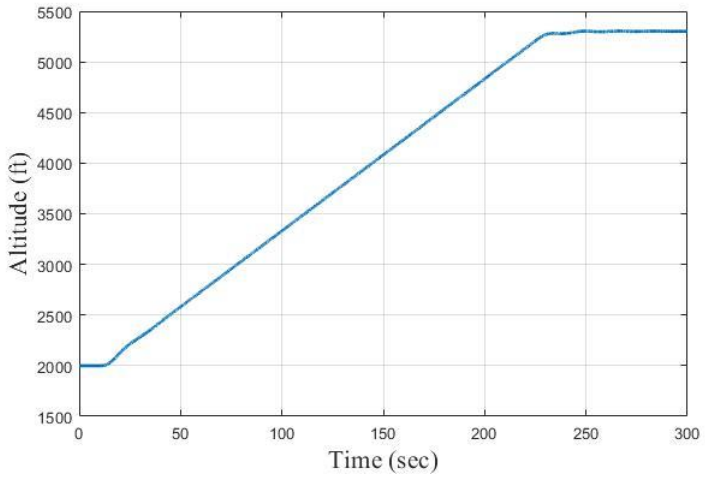

(a) Altitude vs. Time

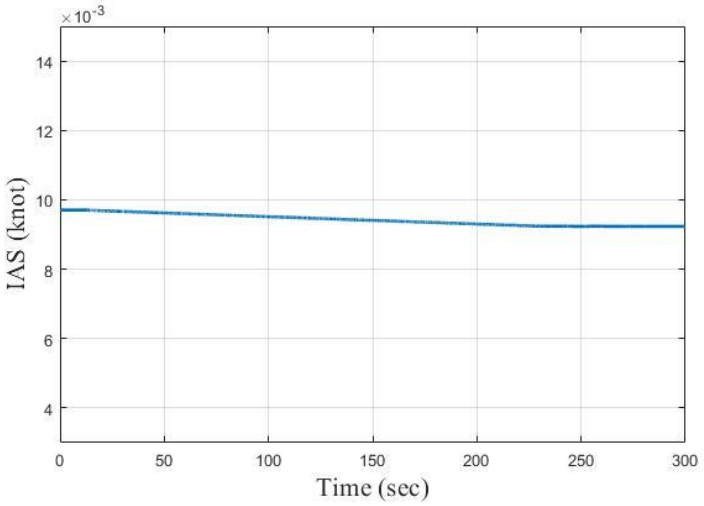

(b) IAS vs. Time

Figure 4.1. Trimming of UH-60 helicopter model with Autopilot, 1st condition: hover at 5370 ft.

Autopilot results for the first trim condition, hover at 5370 ft., for 60 seconds are displayed in Figure 4.2. When the model is started with the trim points of AFCS, SAS modes left “ON” position.

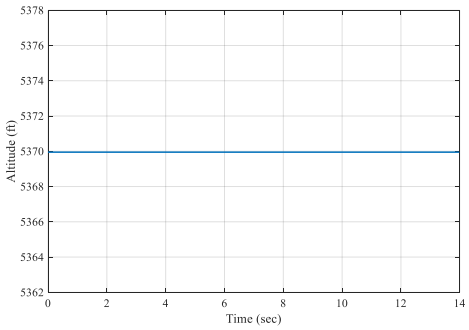

(a) Altitude vs Time

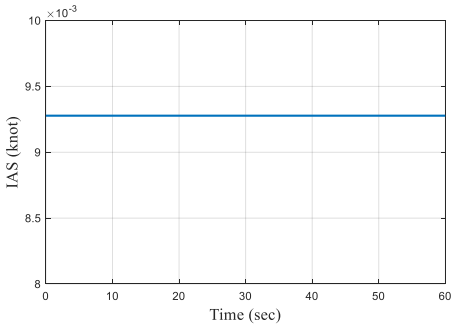

(b) IAS vs Time

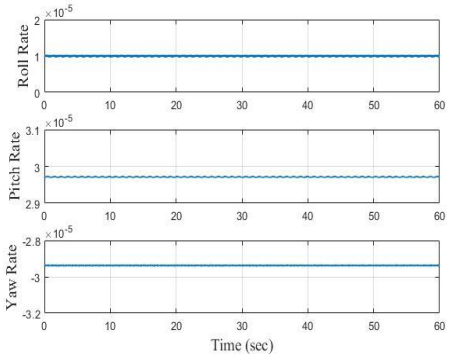

(c) Angle rates (deg/s) vs Time

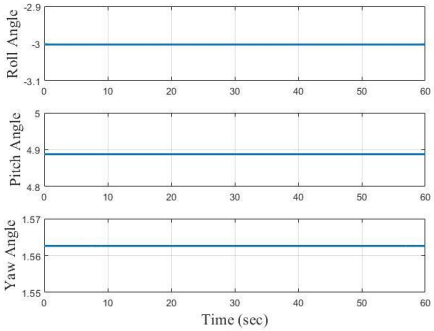

(d) Euler Angles (deg) vs Time

Figure 4.2. Autopilot (AFCS) trim data "SAS ON" for UH-60 helicopter model, 1st condition: hover at 5370 ft.

When autopilot is "OFF", the simulation results for first trim condition are presented in Figure 4.3. It can be seen that the flight conditions do not sail in the first 10 seconds. Since the changes in angular velocity cannot be controlled without SAS controller, the oscillations after ten seconds are inevitable.

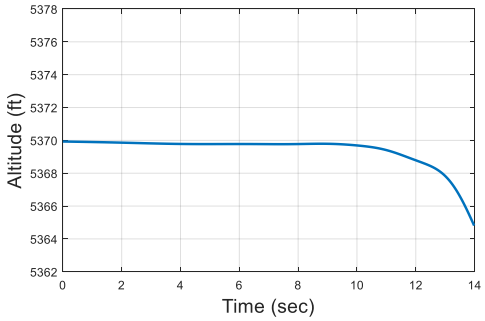

(a) Altitude vs Time

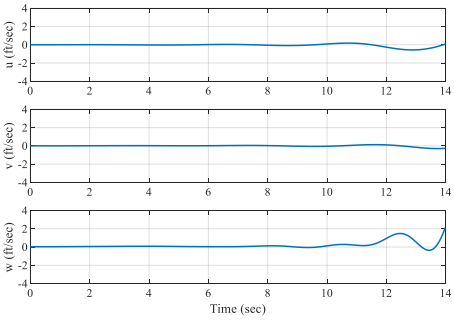

(b) IAS vs Time

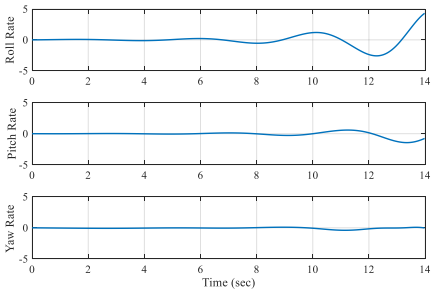

(c) Angle rates (deg/s) vs Time

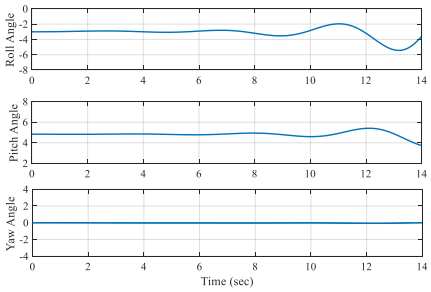

(d) Euler Angles (deg) vs Time

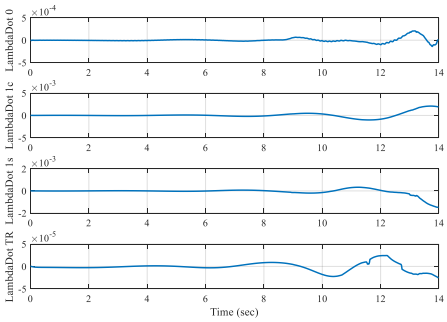

(e) Inflow rates vs Time

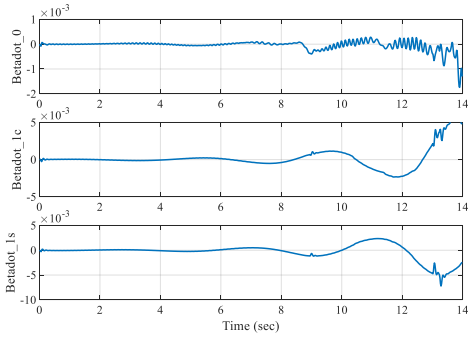

(f) Flapping rates (deg/s) vs Time

Figure 4.3. Autopilot (AFCS) trim data “SAS OFF” for UH-60 helicopter model, 1st condition: hover at 5300 ft.

The variation of cost function versus number of iterations for the first trim condition is given in Figure 4.4.a. Data are obtained by running STE script with the assumptions mentioned in section 3.3.2. The variation of cost function, which is obtained by randomly chosen values for all initial parameters, is given in Figure 4.4.b. The random variables and their range are given in table 4.1. It is observed that the change of initial values does not affect the result of trim solution of STE, but it increases the iteration numbers.

Table 4.1. *List of random variables*

Variable Name:	Min. Value	Max. Value	Unit
α_S	0	10	deg
β_{1S}	0	10	deg
β_{1C}	0	10	deg
θ_{1S}	0	10	deg
λ	0.1	10	deg

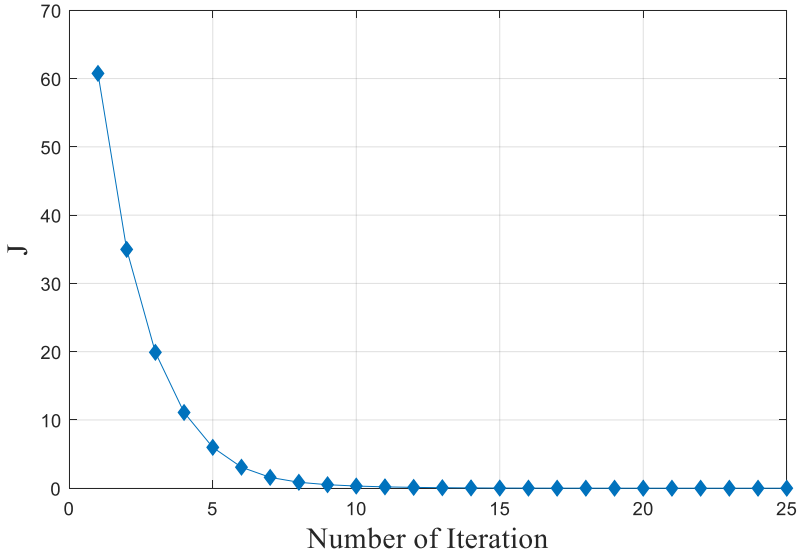

(a) Default value

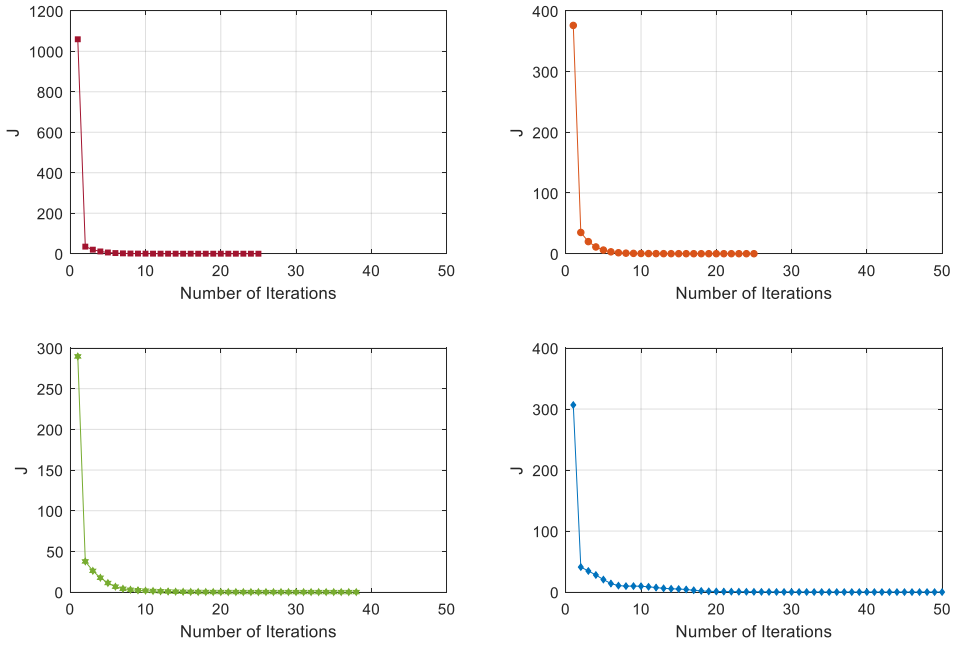

(b) Random values

Figure 4.4. Cost Function (J) of STE vs Number of Iterations, 1st condition: hover at 5300 ft.

The simplex script is executed by using trim conditions obtained by STE simulations. Cost function values of this execution are given in Figure 4.5.a. The results of simplex by random values are given in Figure 4.5.b. It is observed that the system is trapped in a local minimum with the random value set.

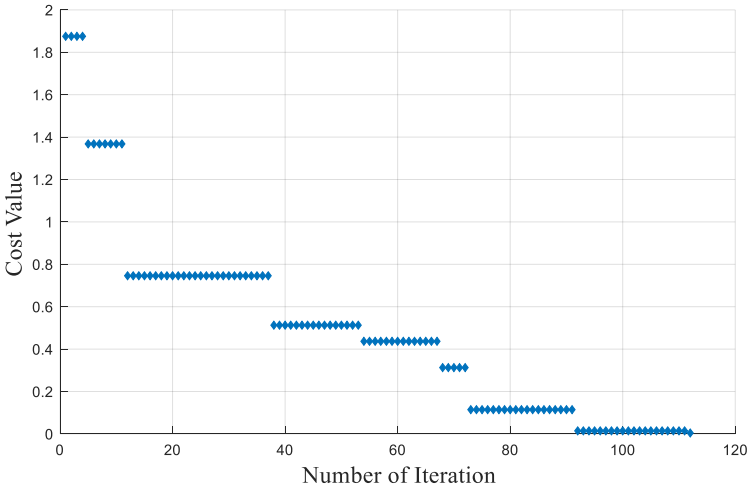

(a) Started with STE results

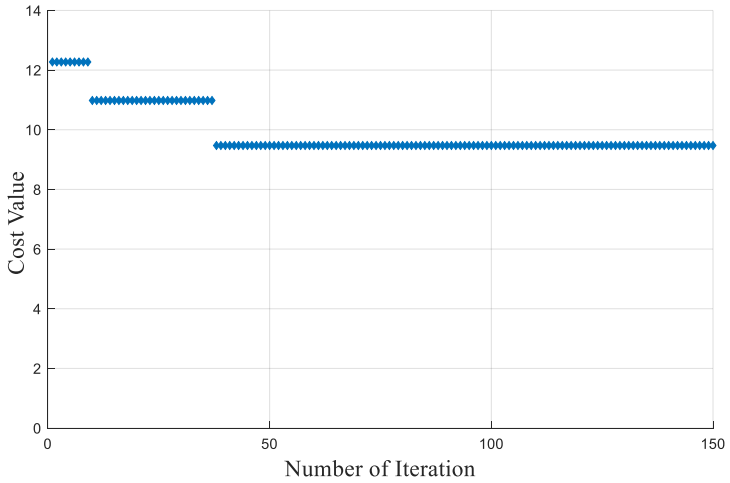

(b) Started with random values

Figure 4.5. Cost Value of NM Simplex Method vs Number of Iterations, 1st condition: hover at 5300 ft.

Table 4.1 gives the trim points for GENHEL [33] and AFCS runs and the trim results for STE and Simplex simulations. It can be observed that the model yields satisfactory results for trim.

Table 4.2. *Comparison of trim results for the 1st trim condition: hover at 5300 ft.*

	GENHEL	AFCS	STE	NM Simplex
Coll (inch)	5.70	5.70	6.18	5.70
Cyc Lat (inch)	0.40	0.42	0.38	0.41
Cyc Long (inch)	0.20	0.27	0.42	0.26
Pedal (inch)	-1.40	-1.36	-1.70	-1.36
Phi (deg)	-3.00	-3.00	-4.10	-3.00
Theta (deg)	5.00	4.87	0	4.88
IAS (knot)	0	0	0	0
Altitude (ft)	5370	5370	5370	5370
p (deg/s)	0	0	0	0
q (deg/s)	0	0	0	0
r (deg/s)	0	0	0	0

Throughout Figure 4.1 it can be observed that the model yields satisfactory results for trim. The velocities and Euler angles fully satisfy the trim condition. There are minor oscillations observed in roll rate (p), pitch rate (q) and yaw rate (r) states. The SAS mode is "ON" when the system is operated, these oscillations thereby have no negative effect on trim condition.

GENHEL and AFCS results are in good agreement for hover at 5370 ft. Comparison of the AFCS parameter values with the GENHEL parameter values gives a good

support for the reliability of the U-60 helicopter model. The comparison of AFCS and GENHEL results shows that the model is validated within certification limitations [34]. Having confidence in the model the AFCS results can be taken as the target data for the trimming by the STE and NM Simplex simulations.

Some differences are observed between AFCS and STE trim results. Some deviations were already expected due to the assumptions made to simplify the equation set. The largest differences are observed for collective and longitudinal cyclic parameters. The angle of theta is zero since the angle of θ_{FP} is assumed as zero while applying the method. We are however not deterred by the differences between the AFCS and STE results. The real purpose of STE simulation is not to determine the exact trim point, instead is to offer a good starting point for Simplex simulations. Viewed in this focus the STE parameter set given in Table 4.2 is considered as a good initial set for Simplex simulations.

Although convergence is good, there are still some differences between procedure (Simplex started with STE output) and AFCS trim results. At this point, the model is run with trim parameters found by the procedure. Runs based on AFCS and procedure ("Simplex") trim parameters are compared in Figure 4.6. It is observed that the differences between these trim parameters do not affect the duration to stay in equilibrium

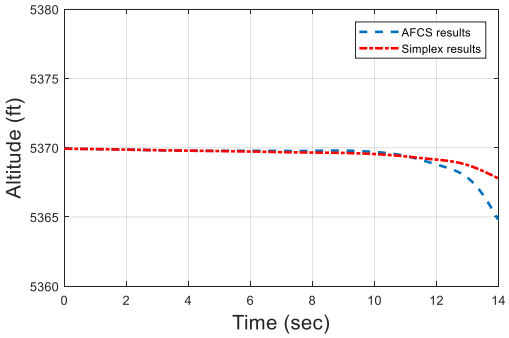

(a) Altitude vs Time

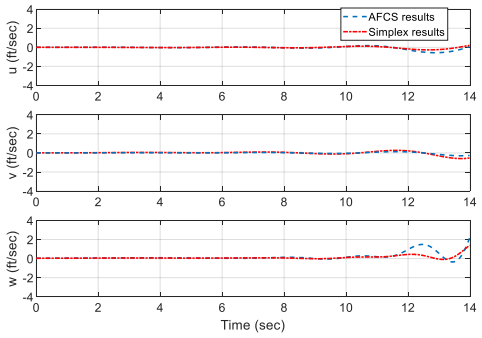

(b) IAS vs Time

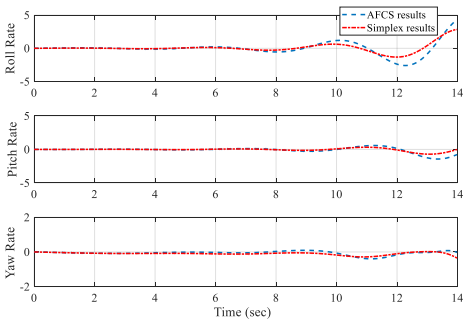

(c) Angle rates (deg/s) vs Time

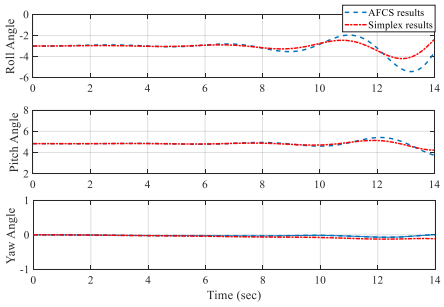

(d) Euler Angles (deg) vs Time

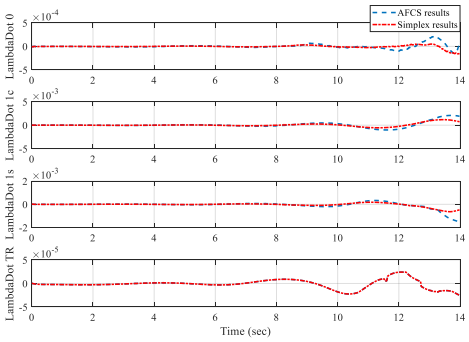

(e) Inflow rates vs Time

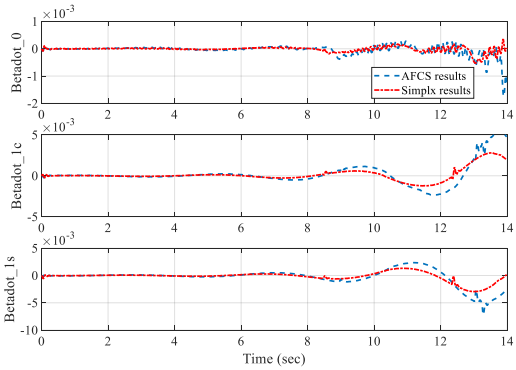

(f) Flapping rates (deg/s) vs Time

Figure 4.6. Comparison the results of AFCS and procedure for UH-60 helicopter model, 1st condition: hover at 5300 ft.

For the second trim point, the model is started with 5300 ft. hover and moved to 5020 ft. 55 knot condition. Speed and altitude information of the simulation are given in Figure 4.7. The reference values are entered to the autopilot at the tenth second. The altitude controller arrived at the target point in about 50 seconds while the speed reached to the target in about 3 minutes. Small fluctuations should be accepted as normal because of the interaction between speed and altitude controllers.

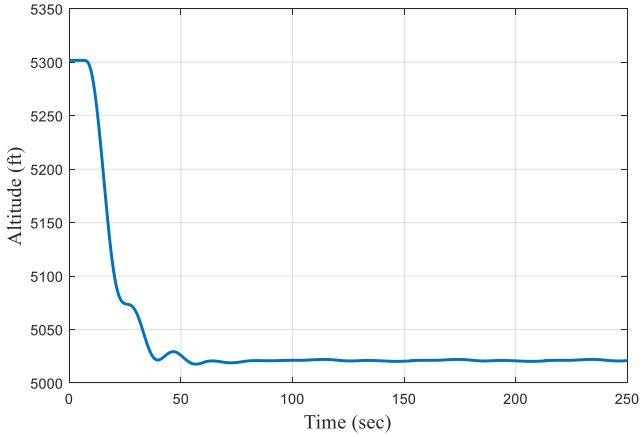

(a) Altitude vs. Time

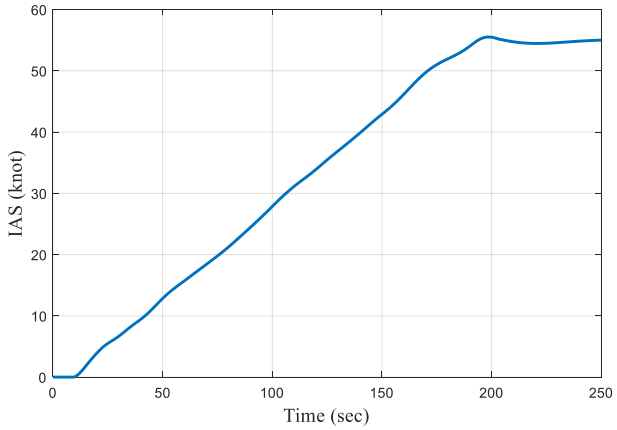

(b) IAS vs. Time

Figure 4.7. Trimming of UH-60 helicopter model with Autopilot, 2nd condition: 55 knot at 5020 ft.

For the second trim point, the system is run at SAS ON condition by using the values obtained with autopilot. The results in 60 seconds are given in Figure 4.8. The SAS controls angle rates reasonably well even if there are some oscillations.

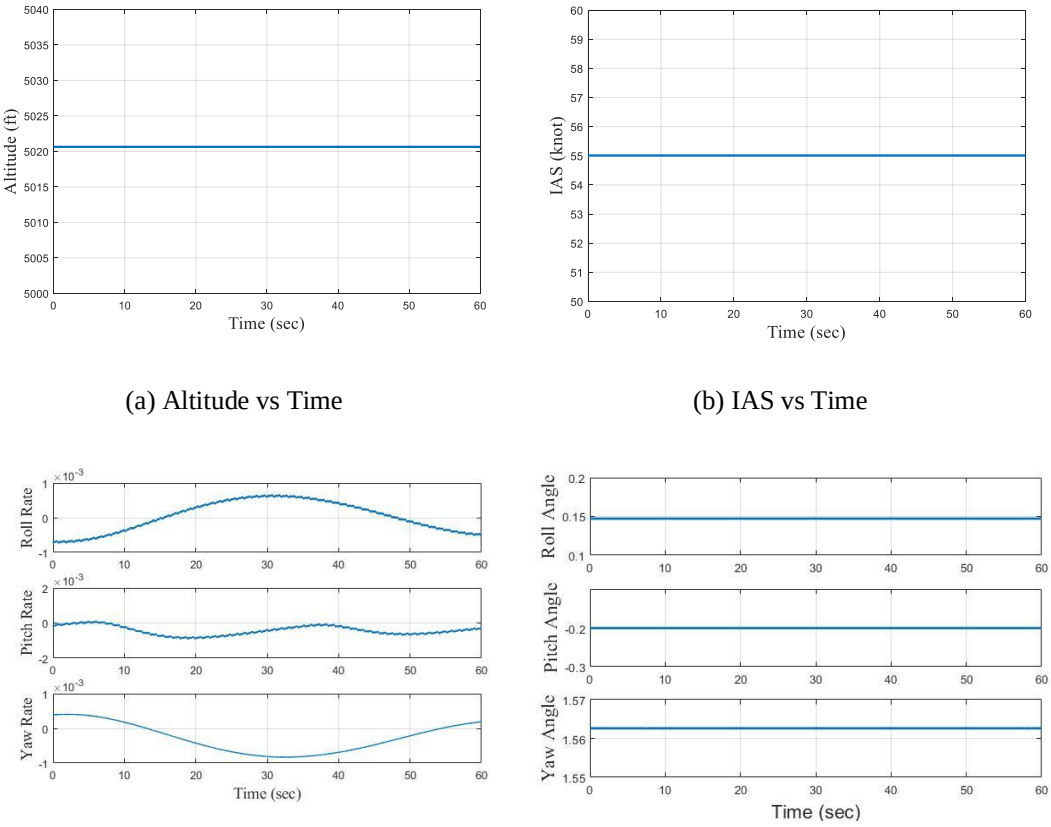

(a) Altitude vs Time

(b) IAS vs Time

(c) Angle rates (deg/s) vs Time

(d) Euler Angles (deg) vs Time

Figure 4.8. Autopilot (AFCS) trim data "SAS ON" for UH-60 helicopter model, 2nd condition: 55 knot at 5020 ft.

When the autopilot is "OFF", simulation results for the second trim condition are represented in Figure 4.9. Flight conditions are maintained for five seconds, which is shorter than that of the first trim condition. The oscillations observed in angle rates

are larger than that of the first condition. Oscillations cause earlier failure without SAS controller.

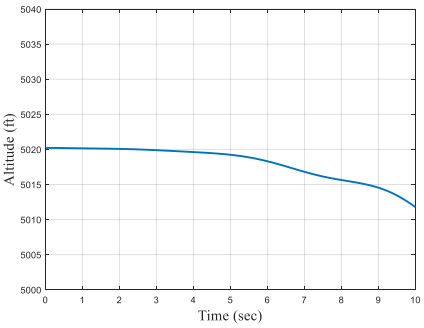

(a) Altitude vs Time

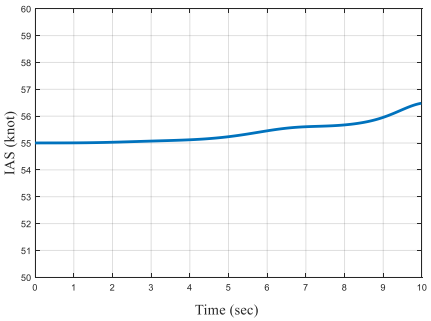

(b) IAS vs Time

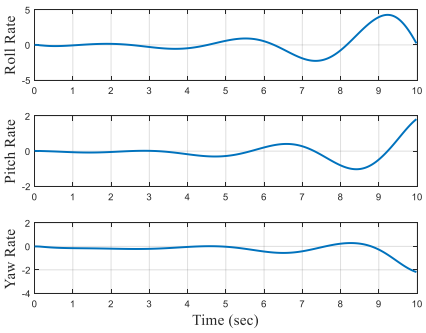

(c) Angle rates (deg/s) vs Time

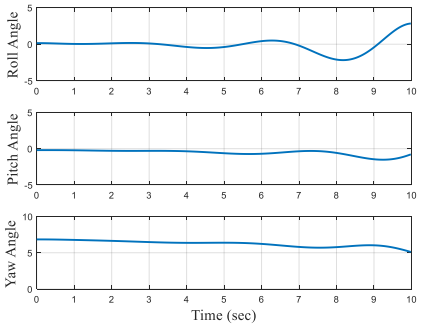

(d) Euler Angles (deg) vs Time

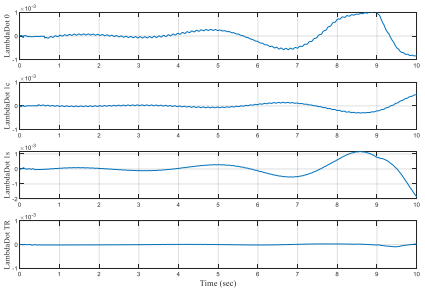

(e) Inflow rates vs Time

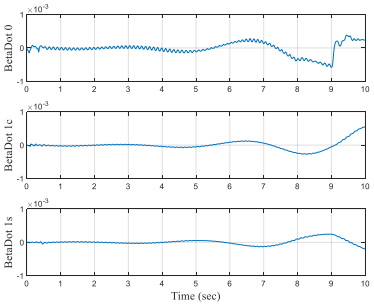

(f) Flapping rates (deg/s) vs Time

Figure 4.9. Autopilot (AFCS) trim data “SAS OFF” for UH-60 helicopter model, 2nd condition: 55 knot at 5020 ft.

The variation of cost function versus number of iterations for the second trim condition is given in Figure 4.10.a. Data are obtained by running STE script with the assumptions mentioned in section 3.3.2. The variation of cost function, which is obtained by randomly chosen values as described above in relation to table 4.1 for all initial parameters, is given in Figure 4.10.b.

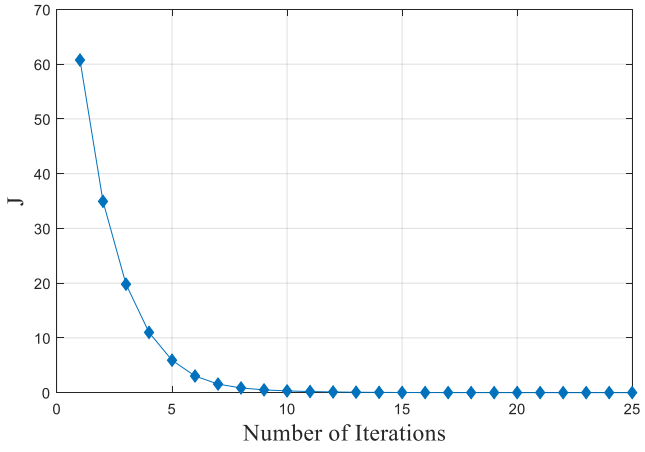

(a) Default value

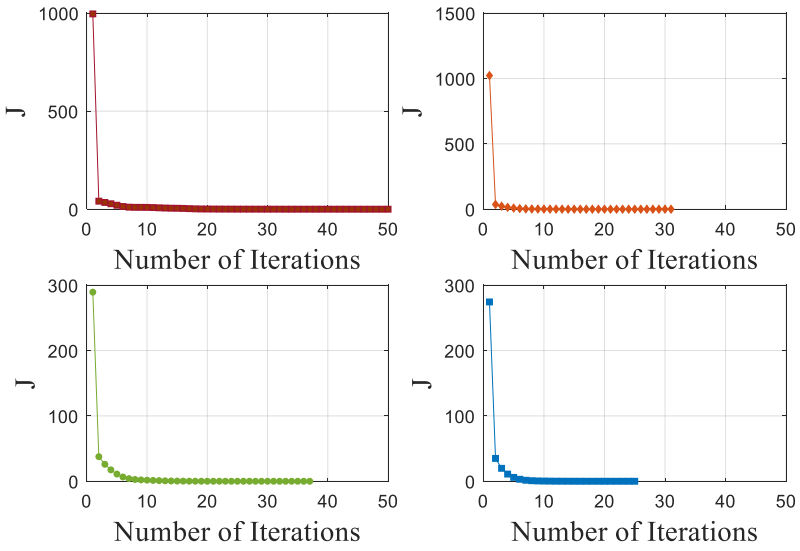

(b) Random values

Figure 4.10. Cost Function (J) of STE vs Number of Iterations, 2nd condition: 55 knot at 5020 ft.

Simplex cost function values, obtained by using the trim set generation of STE simulations, are represented in Figure 4.11.a. Simplex results by using random initial values are given in Figure 4.11.b. As in the first condition, the system gets trapped in a local minimum.

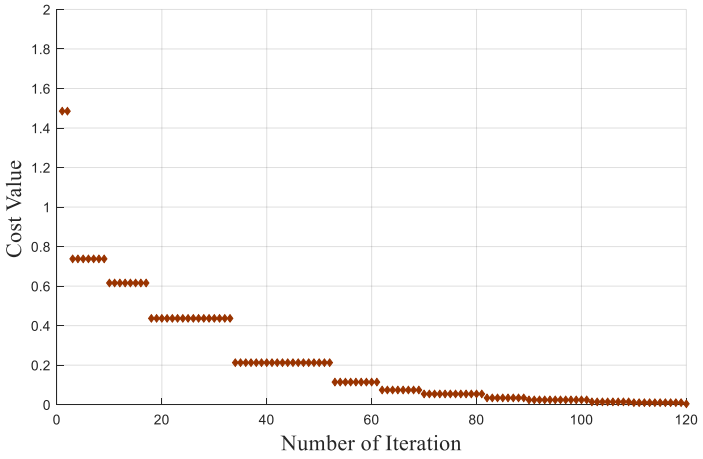

(a) Started with STE results

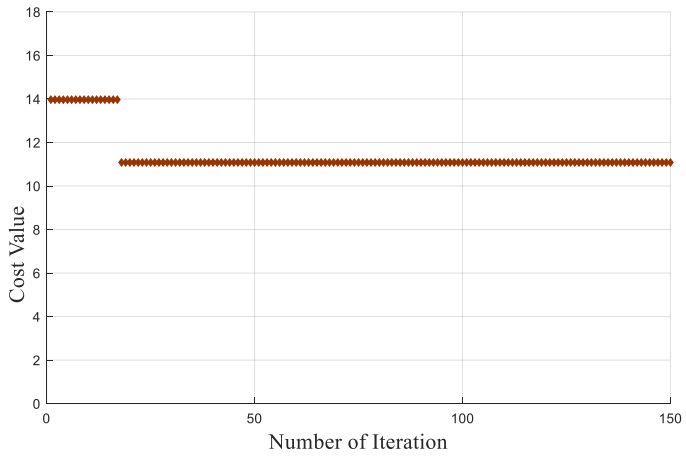

(b) Started with random values

Figure 4.11. Cost Value of NM Simplex Method vs Number of Iterations, 2nd condition: 55 knot at 5020 ft.

Table 4.3 gives the trim points for GENHEL and AFCS runs and the trim results for STE and Simplex simulations. It can be observed that the model yields satisfactory results for trim.

Table 4.3. *Comparison of trim results for the 2nd condition: 55 knot at 5020 ft.*

	GENHEL	AFCS	STE	NM Simplex
Coll (inch)	4.50	4.4	4.7	4.4
Cyc Lat (inch)	0.50	0.55	0.33	0.55
Cyc Long (inch)	0.50	0.57	0.77	0.57
Pedal (inch)	0.20	0.05	0.18	0.05
Phi (deg)	0.50	0.15	-0.07	0.15
Theta (deg)	0.00	-0.20	0	-0.20
IAS (knot)	54.6	55	55	55
Altitude (ft)	5020	5020	5020	5020
p (deg/s)	0	0	0	0
q (deg/s)	0	0	0	0
r (deg/s)	0	0	0	0

For the third trim point, the model is started with 5000 ft 55 knot and moved to 6450 ft 94 knot condition by autopilot. Speed and altitude information of the simulation are given in Figure 4.12. The reference values are entered to the autopilot at the tenth second. The altitude controller arrived at the target point in about 100 seconds while it took the speed to reach the target 30 seconds longer.

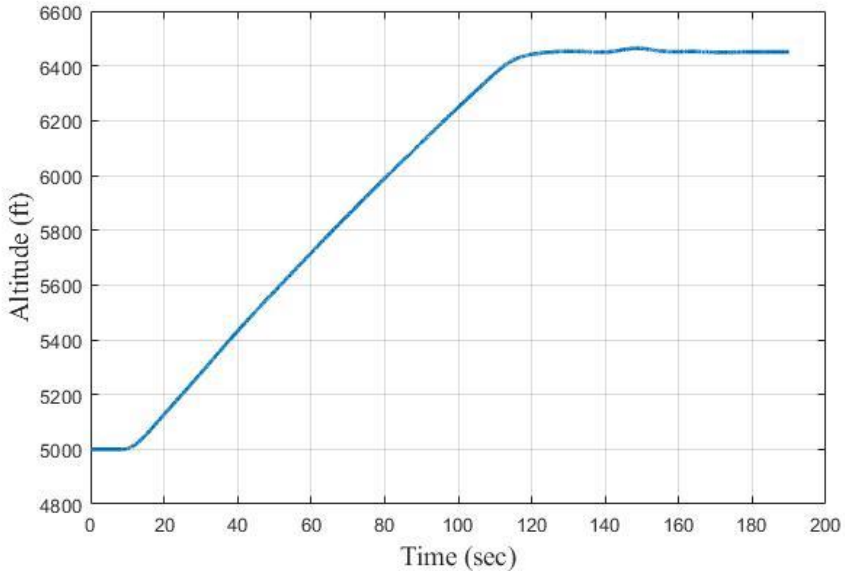

(a) Altitude vs. Time

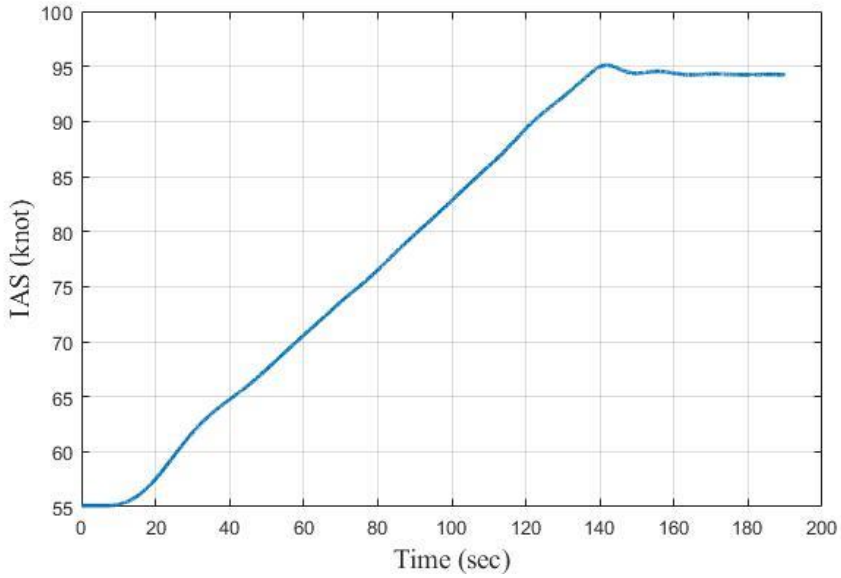

(b) IAS vs. Time

Figure 4.12. Trimming of UH-60 helicopter model with Autopilot, 3rd condition: 93 knot at 6450 ft.

For the third trim point, the system is run at SAS ON condition by using the values obtained with autopilot. The results in 60 seconds are given in Figure 4.13. The SAS controls angle rates reasonably well even if there are some oscillations.

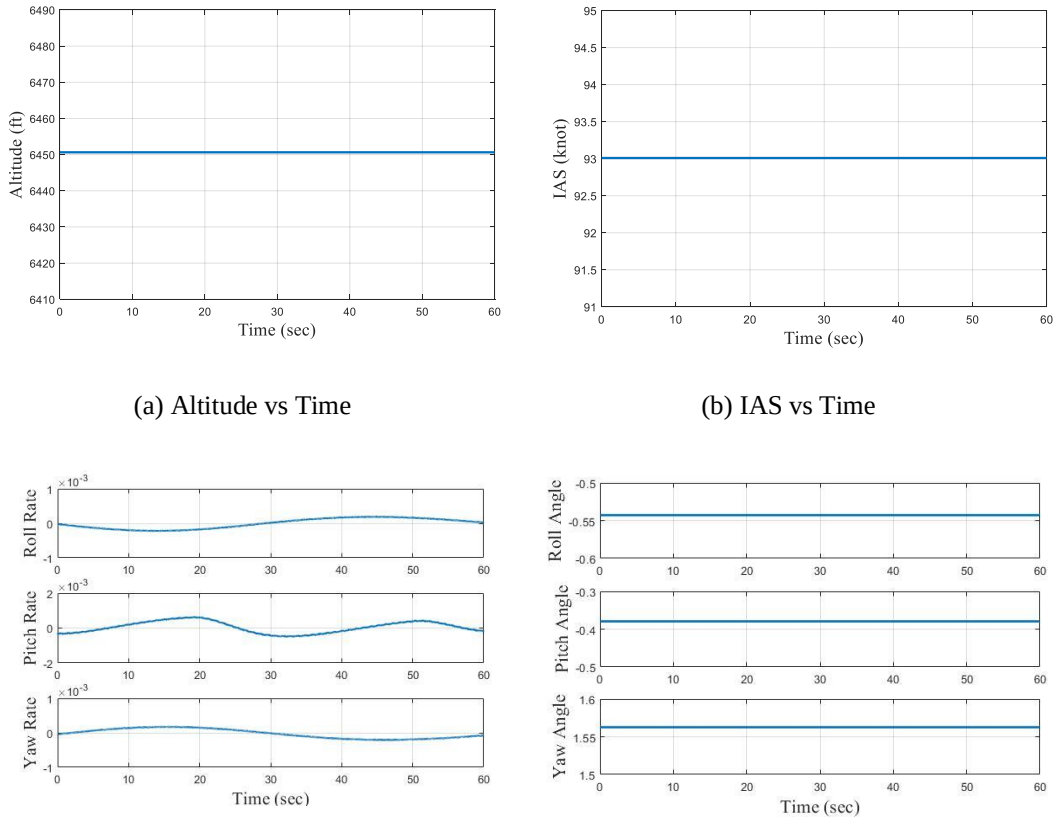

(a) Altitude vs Time

(b) IAS vs Time

(c) Angle rates (deg/s) vs Time

(d) Euler Angles (deg) vs Time

Figure 4.13. Autopilot (AFCS) trim data "SAS ON" for UH-60 helicopter model, 3rd condition: 93 knot at 6450 ft.

When the autopilot is "OFF", simulation results for the third trim condition are given in Figure 4.14. Flight conditions are maintained for about six seconds. Oscillations cause earlier failure without SAS controller.

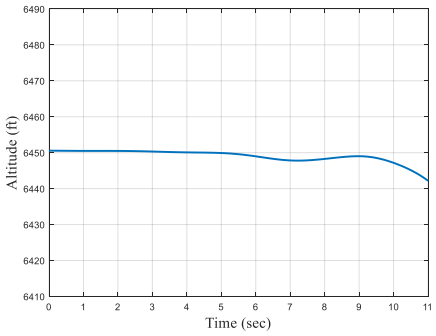

(a) Altitude vs Time

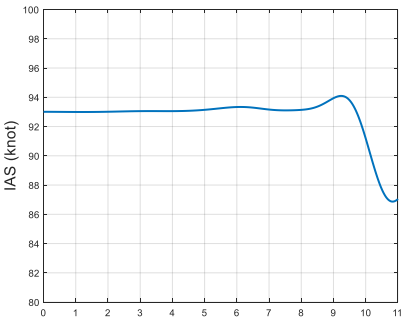

(b) IAS vs Time

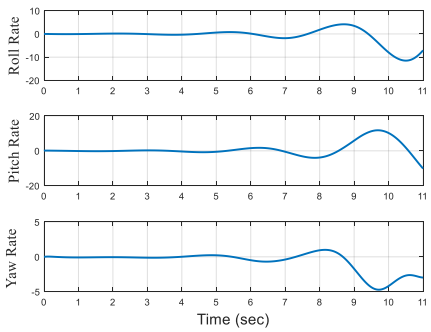

(c) Angle rates (deg/s) vs Time

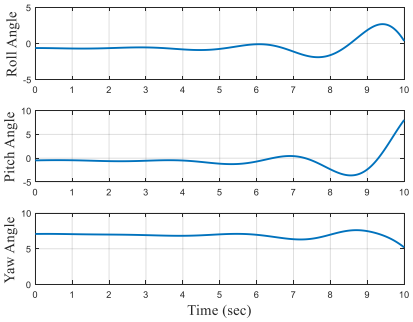

(d) Euler Angles (deg) vs Time

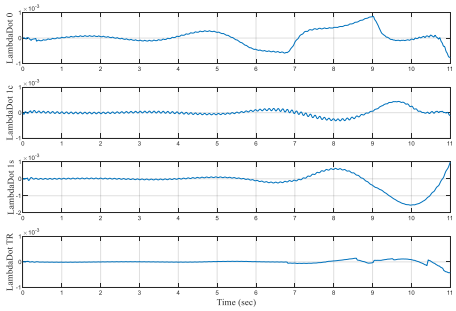

(e) Inflow rates vs Time

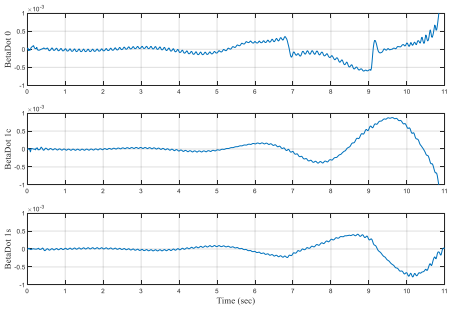

(f) Flapping rates (deg/s) vs Time

Figure 4.14. Autopilot (AFCS) trim data “SAS OFF” for UH-60 helicopter model, 3rd condition: 93 knot at 6450 ft.

The variation of cost function versus number of iterations for the third trim condition is given in Figure 4.15.a. Data are obtained by running STE script with the assumptions mentioned in section 3.3.2. The variation of cost function, which is obtained by randomly chosen values as described above in relation to table 4.1 for all initial parameters, is given in Figure 4.15.b.

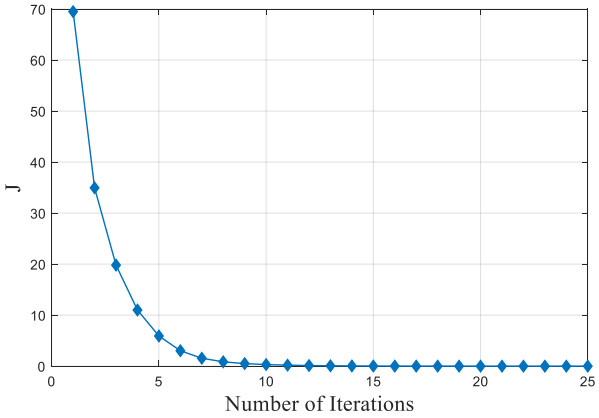

(a) Default value

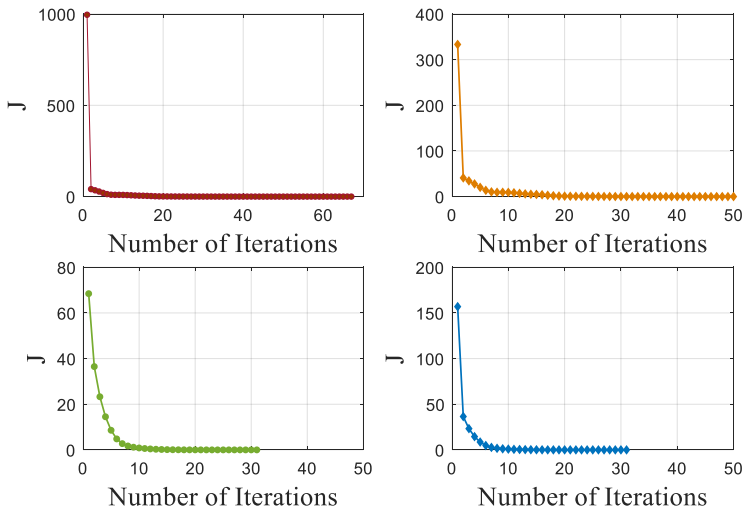

(b) Random values

Figure 4.15. Cost Function (J) of STE vs Number of Iterations, 3rd condition: 93 knot at 6450 ft.

Simplex cost function values, obtained by using the trim set generation of STE, are represented in Figure 4.16.a. Simplex results by using random initial values are given in Figure 4.16.b. As in the previous conditions, the system gets trapped in a local minimum.

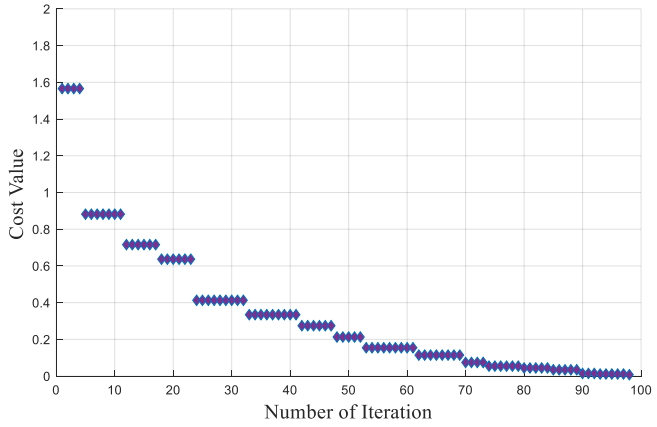

(a) Started with STE results

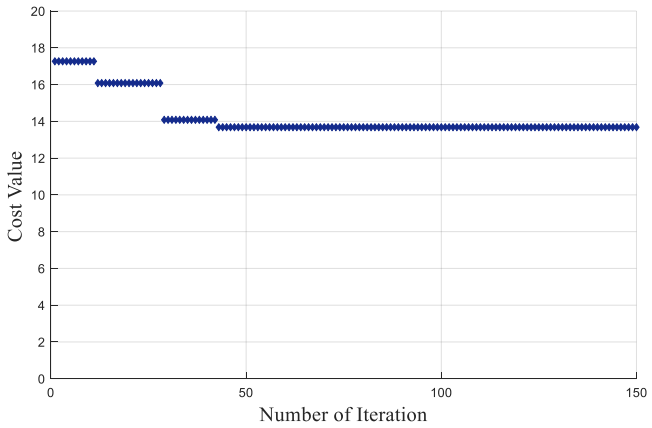

(b) Started with random values

Figure 4.16. Cost Value of NM Simplex Method vs Number of Iterations, 3rd condition: 93 knots at 6450 ft.

Table 4.4 gives the trim points for GENHEL and AFCS runs and the trim results for STE and Simplex simulations. It can be observed that the model yields satisfactory results for trim.

Table 4.4. *Comparison of trim results for the 3rd condition: 93 knots at 6450 ft.*

	GENHEL	AFCS	STE	NM Simplex
Coll (inch)	5.00	4.90	5.08	4.90
Cyc Lat (inch)	0.50	0.59	0.47	0.59
Cyc Long (inch)	-1.00	-0.88	-0.74	-0.88
Pedal (inch)	0.60	0.40	0.5	0.40
Phi (deg)	0.00	-0.54	-0.61	-0.54
Theta (deg)	0.00	-0.38	0	-0.38
IAS (knot)	92.8	93	93	93
Altitude (ft)	6450	6450	6450	6450
p (deg/s)	0	0	0	0
q (deg/s)	0	0	0	0
r (deg/s)	0	0	0	0

The examination of the results for the three different flight conditions shows that the model obtains better trim points at lower speeds. While the speed increases, oscillations start in angle rates. Thus, flight conditions of the aircraft break up more quickly at the obtained trim points. But all these three conditions should be assessed as acceptable with their behaviors to the generation without autopilot. The NM simplex method also found the same result with autopilot by two significant figures under these three trim conditions.

Furthermore, the procedure is tested for two points that cannot be trimmed by autopilot: 10 knot backward speed at 2000 ft. and 20 knots lateral speed at 2000 ft.

When the autopilot is “OFF”, simulation results for 10 knots backward speed at 2000 ft. condition are represented in Figure 4.17. Flight conditions are maintained for four seconds since this condition is extreme.

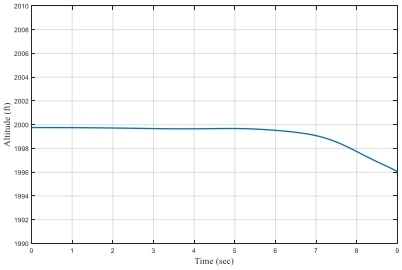

(a) Altitude vs Time

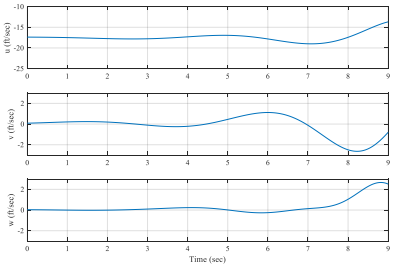

(b) IAS vs Time

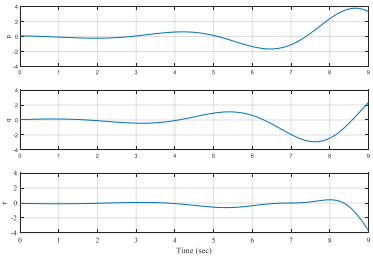

(c) Angle rates (deg/s) vs Time

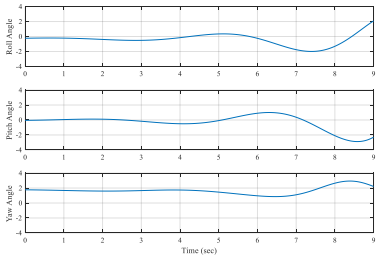

(d) Euler Angles (deg) vs Time

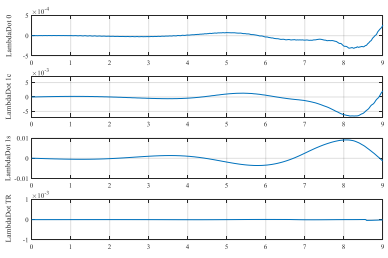

(e) Inflow rates vs Time

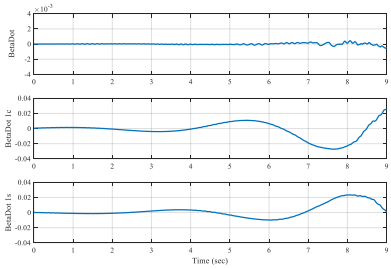

(f) Flapping rates (deg/s) vs Time

Figure 4.17. Trim data “SAS OFF” for UH-60 helicopter model, 4th condition: 10 knots backward speed at 2000 ft.

When the autopilot is “OFF”, simulation results for 20 knots lateral speed at 2000 ft. condition are represented in Figure 4.18. Flight conditions are maintained for three seconds since this condition is extreme.

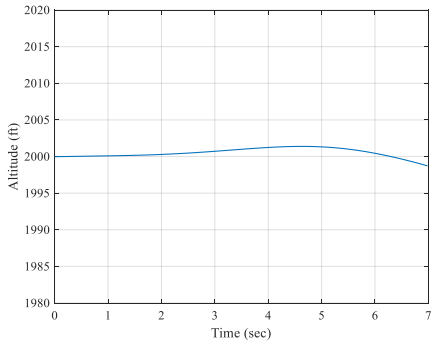

(a) Altitude vs Time

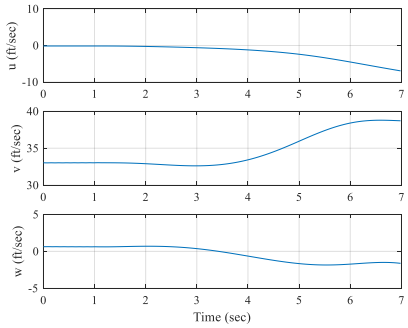

(b) IAS vs Time

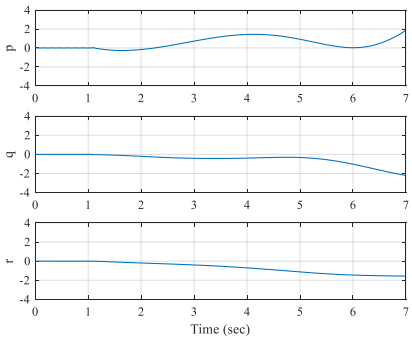

(c) Angle rates (deg/s) vs Time

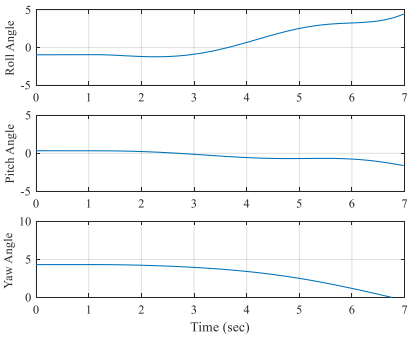

(d) Euler Angles (deg) vs Time

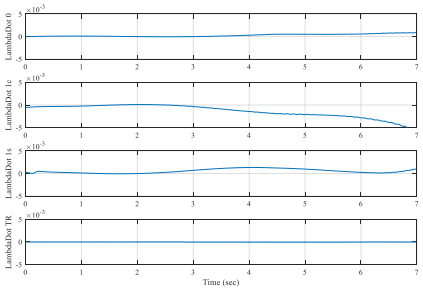

(e) Inflow rates vs Time

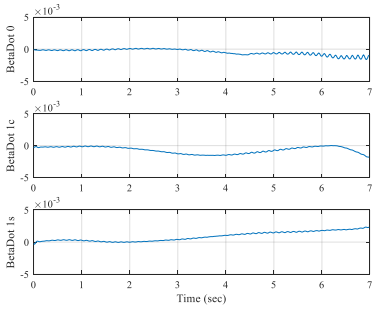

(f) Flapping rates (deg/s) vs Time

Figure 4.18. Trim data “SAS OFF” for UH-60 helicopter model, 5th condition: 20 knot lateral speed at 2000 ft.

CHAPTER 5

CONCLUSIONS AND FUTURE WORK

In this thesis, the development and the application of a procedure that can find trim points for a helicopter flight model with reasonable assumptions is described. In principle, this procedure can be applied to any specified helicopter design throughout the flight envelope.

A helicopter (UH-60) model based on reference [1] is used to find the target trim points using an autopilot. Later, a procedure is defined to reach trim without using autopilot. The procedure consisted of two MATLAB scripts acting in serial that are generated by implementing Fixed-Point Iteration and NM Simplex methods.

The procedure makes use of two advantages of the NM method and eliminates one disadvantage. One of the advantages of NM method is that it is computationally inexpensive since it does not require any derivative information. The second advantage is that it gives results without restrictive assumptions on the flight model. This is shown by the agreement of the procedure results with that of the autopilot results. The convergence of the NM method, has a dependence on the initial values. This is handled by first solving a set of Simplified Trim Equations (STE) set and generating initial values for the NM iteration.

The reliability of the assumptions is tested for trimming the UH-60 helicopter at different altitude-speed conditions. The trim analysis results are compared with real flight test data. This comparison showed that the simulation results agree with the test data within acceptable limits for pilot training at various altitude-speed conditions.

The results at three different flight conditions showed that the model obtains better results in finding trim points at lower speeds. In finding trim points at higher forward speeds, oscillations in angle rates are observed when the defined procedure is used. Such deficiencies result in the divergence of the model after about 10 seconds. Results obtained by the defined procedure and the autopilot are within two significant figures for the tested conditions. To obtain closer results, the weighting vector in the cost function can be further updated.

The procedure is further tested for two points that cannot be trimmed by autopilot. The flight conditions are chosen at sideward speed and backward speeds. Thereby, it is demonstrated that while it is not possible to find trim conditions with an autopilot that is not designed for those flight conditions, it can be found with the defined procedure. Therefore, it can be suggested that the procedure can be useful in the design process of a helicopter and its autopilot. For example, the calculation of trim conditions is important in the analysis of helicopter flight dynamics and stability. Furthermore, automatic flight control systems are designed and evaluated at trim conditions. In addition, different models of aircraft are compared by using their trim conditions and also models are compared with flight data according at trim points.

There are several possibilities to extend and to improve the procedure developed in this thesis. One of the possibilities is to include further model components to the flight model, such as a model of a landing gear, ground effect, etc. That way, one can also work on trimming close to the ground. Another extension is to include an engine model. By doing so the effects of engine parameters on trimming can be examined. It would also be practical to prepare a user-friendly graphical interface.

REFERENCES

[1] J. J. Howlett, UH-60A Black Hawk Engineering Simulation Program. Volume 1: Mathematical Model Final Report (Sikorsky Aircraft, Stratford, Conn.), December 1981

[2] Howlett, J. J., "UH-60A Black Hawk Engineering Simulation Program—Volume II Background Report," NASA CR-166310, Dec. 1981.

[3] Peters, D.A., and Barwey, D., "A General Theory of Rotorcraft Trim," Proceedings of the 36th AIAA/ASME/ASCE/AHS/ASC Structures, Structural Dynamics and Materials Conference, New Orleans, LA, April 1995, Paper No. 95-1451, pp. 2558-2595.

[4] Wheatley, J.B., "An Aerodynamic Analysis of the Autogiro Rotor with a Comparison Between Calculated and Experimental Results," NACA Report No. 487, January 1934.

[5] Peters, D.A., and Ormiston, R.A., "Flapping Response Characteristics of Hingeless Rotor Blades by a Generalized Harmonic Balance Method," NASA TN D-7856, February 1975.

[6] Eipe, Abraham, Effect of Some Structural Parameters on Elastic Rotor Loads by an Iterative Harmonic Balance, Doctor of Science Thesis, Washington University in St. Louis, December 1979.

[7] Yen, J. G., Corrigan, J. J., Schillings, J. J., & Hsieh, P. Y. (1994, January). Comprehensive analysis methodology at bell helicopter: COPTER. In Proceedings of the American Helicopter Society Aeromechanics Specialists Conference.

[8] Peters, D. A., arid Izadpanah, A., "Helicopter Trim by Periodic Shooting with Newton - Raphson Iteration j" Paper 81-23, Proceedings of the 37th Annual National Forum of the American Helicopter Society, Alexandria, VA, May 1981.

[9] O'Malley, J. A., Izadpanah, A.P. and Peters, D. A., "Comparisons of Three Numerical Trim MEthods for Rotro Air Loads" Proceedings of the Ninth European Rotorcraft Forum, Italy, Sepember 13-15,1983, Paper No. 58

[10] Achar, N.S., and Gaonkar, G.H., "Helicopter Trim Analysis by Shooting and Finite Element Methods with Optimally Damped Newton Iterations," AIAA Journal, Vol. 31, No. 2, February 1993.

[11] Peters, M.H., and Peters, D.A., "Discrete Control Theory and Dynamic Observers Applied to Rotorcraft Stability and Trim," Presented at the 54th AHS Forum, Washington, D.C., May 20-22, 1998.

[12] Lim, J. W., & Chopra, I. (1990). Stability sensitivity analysis of a helicopter rotor. AIAA journal, 28(6), 1089-1097.

[13] Peters, D. A., and Izadpanah, A. P., hp-version finite elements for the space-domain, Computational Mechanics, 3, (1988), 73-88

[14] Peters, D. A., Kirn, B. S., and Chen, H.-S., "Calculation of Trim Settings of a Helicopter Rotor by an Optimized Automatic Controller," Journal of Guidance, Control, and Dynamics, Vol. 7, No. 1, 1984, pp. 85-91.

[15] Peters, D.A., Bayly, P., and Li, S., "A Hybrid Periodic-Shooting, Autopilot Method for Rotorcraft Trim Analysis," Proceedings of the 52nd AHS Forum, Washington D.C., June 4-6, 1996.

[16] Friedman, C., & Rand, O. (2008). A Highly Robust Trim Procedure for Rotorcraft Simulations. In AIAA Modeling and Simulation Technologies Conference and Exhibit (p. 6361).

[17] Enns, Russell, and Si, Jennie, "Helicopter Trimming and Tracking Control Using Direct Neural Dynamic Programming," IEEE Transactions on Neural Networks, Vol. 14, No. 4, July 2003.

[18] Riviello, Luca, Rotorcraft Trim by a Neural Model-Predictive Auto-Pilot, M.s Thesis, Georgia Institute of Technology, April 2005.

[19] Wang, W., Li, D., & Liu, C. (2019). Helicopter flight simulation trim in the coordinated turn with the hybrid genetic algorithm. Proceedings of the Institution of Mechanical Engineers, Part G: Journal of Aerospace Engineering, 233(3), 1159-1168.

[20] Dai, J., Wu, G., Wu, Y., & Zhu, G. (2008, June). Helicopter trim research based on hybrid genetic algorithm. In 2008 7th World Congress on Intelligent Control and Automation (pp. 2007-2011). IEEE.

[21] Mark E. Dreier, "Introduction to Helicopter and Tiltrotor Flight Simulation," AIAA Education Series, 2007.

[22] Lee, D., Sezer-Uzol, N., Horn J. F., and Long, L. N., "Simulation of Helicopter Shipboard Launch and Recovery with Time-Accurate Airwakes," *Journal of Aircraft,*Vol. 42, No. 2, 2005, pp. 448–461.

[23] Horn J. F., and Sahani, N., "Detection and Avoidance of Main Rotor Hub Moment Limits on Rotorcraft," *Journal of Aircraft,*Vol. 41, No. 2, 2004, pp. 372–379.

[24] Ballin, M. G. (1991). Validation of the dynamic response of a blade-element UH-60 simulation modelin hovering flight. *Journal of the American Helicopter Society,* 36(4), 77-88

[25] K. Braman, S. Ramachadran, "Helicopter Simulation Techniques For Full Mission Flight Simulation," I/ITSEC, 1986.

[26] J. Gordon Leishman, "Principles of Helicopter Aerodynamics," Cambridge Aerospace Series, Second Edition, 2006.

[27] Pitt D. M. and Peters D. A. "*Theoretical Prediction of Dynamic - Inflow Derivatives*", Vertica Vol. 5, 1981.

[28] Pitt D. M. and Peters D. A. "*Rotor Dynamic Inflow Derivatives and Time constants from Various Inflow Models*", 9th European Rotorcraft Forum Paper No:55, Italy, September, 1983.

[29] Burden, R. L. & Faires, J. D. (2010). Numerical Analysis, Ninth Edition Brooks-Cole. Boston, Mass, USA.

[30] Wayne Johnson, "Rotorcraft Aeromechanics," Cambridge University Press, 2013.

[31] Yavrucuk, I., "Simplified Trim Equations," lecture notes AE584 at METU, Helicopter Stability and Control, fall 2018

[32] Alonso, J. J. (2010). Aa222: Introduction to multidisciplinary design optimization, "Chapter 6: Gradient-Free Optimization" Lecture Notes. *http://adl.stanford.edu/aa222/lecture_Notes.html* accessed 01/08/2019

[33] Ballin, Mark G. "Validation of a Real-Time Engineering Simulation of the UH-60A Helicopter," February 1987.

[34] Anon, "EASA CS-FSTD (H): Certification Specifications for Helicopter Flight Simulation Training Devices," European Aviation Safety Agency, June 2012.

APPENDICES

A. Mathematical Model of The Main Rotor

The main rotor model is based on a blade element analysis in which total rotor forces and moments are developed from a combination of aerodynamic, mass and inertia loads acting on each blade.

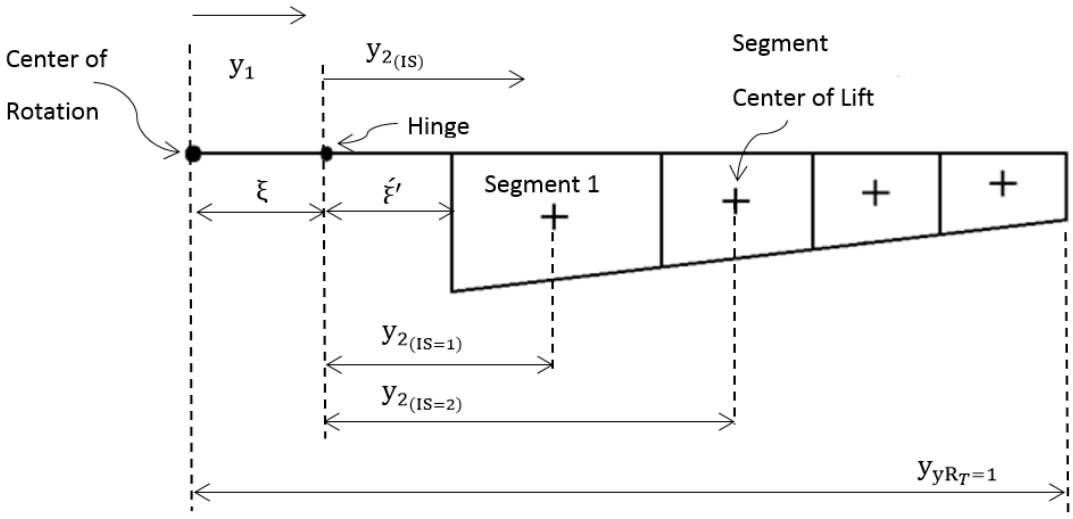

Figure 0.1. Main Rotor Blade Equal Annuli Area Segment Distribution [1]

where “e“ is the hinge offset and ” é “ is the cut-out length and R_T is the rotor radius. Hinge offset and cut-out lengths are normalized by the rotor radius.

$$e = \frac{\xi}{R_T} \qquad (A.1)$$

$$\acute{e} = \frac{\acute{\xi}}{R_T} \tag{A.2}$$

irst segment midpoint “y” location is;

$$y_{21} = \left\{\left[\frac{1-(e+\acute{e})^2}{2*NSS}\right] + (e+\acute{e})^2\right\}^{1/2} - e \tag{A.3}$$

where NSS is number of blade segments.

The midpoints of other segments should be determined by,

$$y_{2_{IS}} = \left\{\left[\frac{1-(e+\acute{e})^2}{NSS}\right] + \left(e + y_{2_{IS-1}}\right)^2\right\}^{1/2} - e \tag{A.4}$$

where IS means indicating segment. The segments “y” locations should be obtained by this equation above except first blade segment. After definitions of “y” locations, the segment widths will be,

$$\Delta y_{IS} = y_{outbord_{IS}} - y_{inbord_{IS}} \qquad IS = 1,2,\ldots..NSS \tag{A.5}$$

where,

$$y_{outbord_{IS}} = \left\{\left(y_{2_{IS}} + e\right)^2 + \left[\frac{1-(e+\acute{e})^2}{2*NSS}\right]\right\}^{1/2} \tag{A.6}$$

$$y_{y_{inbord_{IS}}} = \left\{\left(y_{2_{IS}} + e\right)^2 - \left[\frac{1-(e+\acute{e})^2}{2*NSS}\right]\right\}^{1/2} \tag{A.7}$$

and segments mean chord becomes,

$$C_{y_{IS}} = \left[\left(\frac{C_T - C_R}{1-e-\acute{e}}\right)\left(\frac{y_{outbord_{IS}} + y_{inbord_{IS}} - 2(e+\acute{e})}{2}\right)\right] + C_R \tag{A.8}$$

C_T and C_R are tip chord and root chord of the blade respectively. Segment are finally can be calculated by,

$$S_{y_{IS}} = (R_T)\left(C_{y_{IS}}\right)\left(y_{outbord_{IS}} - y_{inbord_{IS}}\right) \quad IS = 1,2,\ldots..NSS \tag{A.9}$$

The total forces acting on the blade are derived from the total velocity components at the blade together with control inputs.

By using $V = \dot{r} + w \times r$ and differentiating the equation for acceleration translational accelerations at the rotor hub becomes,

$$\dot{U}_{Hub} = \dot{U}_{Body} - rV_{Body} + qw_{Body} - X_H(q^2 + r^2) + Y_H(pq - \dot{r}) + Z_H(pr + \dot{q}) + g_x \tag{A.10}$$

$$\dot{V}_{Hub} = \dot{V}_{Body} - pw_{Body} + rU_{Body} + X_H(pq + \dot{r}) - Y_H(p^2 + r^2) + Z_H(qr - \dot{p}) + g_y \tag{A.11}$$

$$\dot{W}_{Hub} = \dot{w}_{Body} - pV_{Body} - qU_{Body} + X_H(pr + \dot{q}) + Y_H(qr + \dot{p}) - Z_H(p^2 + q^2) + g_z \tag{A.12}$$

where g components are gravity components and X_H , Y_H , Z_H are longitudunal, lateral and vertical rotor arms from the CG of the aircraft.

The translational velocities of the rotor hub can be written as

$$\mu_{XH} = \frac{1}{\Omega_T R_T}\{U_{Body} + qZ_H - rY_H\} \tag{A.13}$$

$$\mu_{YH} = \frac{1}{\Omega_T R_T}\{V_{Body} + rX_H - pZ_H\} \tag{A.14}$$

$$\mu_{ZH} = \frac{1}{\Omega_T R_T}\{w_{Body} - qX_H + pY_H\} \tag{A.15}$$

where X_H , Y_H , Z_H are longitudinal, lateral and vertical rotor arms from the CG of the aircraft. Velocity components are normalized by the tip speed of the blades (Advance

ratio). These velocity components and body rates has to be transferred through the shaft axis.

Body to shaft axes transformation matrix is

$$A_{BDSH} = \begin{bmatrix} \cos I_\theta & 0 & -\sin I_\theta \\ \sin I_\theta \sin I_\emptyset & \cos I_\emptyset & \cos I_\theta \sin I_\emptyset \\ \sin I_\theta \cos I_\emptyset & -\sin I_\emptyset & \cos I_\theta \cos I_\emptyset \end{bmatrix} \quad \text{(A.16)}$$

Body translational accelerations at the hub (Shaft axes)

$$\begin{bmatrix} \dot{V}_{XS} \\ \dot{V}_{YS} \\ \dot{V}_{ZS} \end{bmatrix} = A_{BDSH} \begin{bmatrix} \dot{U}_{Hub} \\ \dot{V}_{Hub} \\ \dot{W}_{Hub} \end{bmatrix} \quad \text{(A.17)}$$

Body angular accelerations at the rotor hub (shaft axes)

$$\begin{bmatrix} \dot{p}_s \\ \dot{q}_s \\ \dot{r}_s \end{bmatrix} = A_{BDSH} \begin{bmatrix} \dot{p} \\ \dot{q} \\ \dot{r} \end{bmatrix} \quad \text{(A.18)}$$

Body translational velocities at the hub (Shaft axes)

$$\begin{bmatrix} \mu_{XS} \\ \mu_{YS} \\ \mu_{ZS} \end{bmatrix} = A_{BDSH} \begin{bmatrix} \mu_{XH} \\ \mu_{YH} \\ \mu_{ZH} \end{bmatrix} \quad \text{(A.19)}$$

Body angular velocities at the rotor hub (shaft axes)

$$\begin{bmatrix} p_s \\ q_s \\ r_s \end{bmatrix} = A_{BDSH} \begin{bmatrix} p \\ q \\ r \end{bmatrix} \quad \text{(A.20)}$$

The rotor air mass degree of freedom is primarily based on a uniform downwash distribution developed from rotor thrust by application of momentum theory. This uniform downwash which is passed through a first order lag is modified to account for the changing distribution with forward speed and aerodynamic pitching and rolling moment loading on the rotor. In the first case the resultant uniform downwash is distributed 1st harmonically around the azimuth as a cosine function depending on the

inclination of the rotor wake. So total downwash contribution at the rotor disk U_{PD} becomes,

$$\begin{aligned} U_{PD_I} = & -D_{W0}\cos(\beta_{IB}) \\ & + (D_{WC} \\ & - K_{1X}D_{W0})\cos(\beta_{IB})\left[e\cos(\psi_{IB})\right. \\ & \left. + y_{2_{IS}}\cos(\psi_{IB}+\delta_{IB})\right] + (D_{WS} \\ & + K_{1Y}D_{W0})\cos(\beta_{IB})\left[e\sin(\psi_{IB})\right. \\ & \left. + y_{2_{IS}}\sin(\psi_{IB}+\delta_{IB})\right] \end{aligned} \tag{A.21}$$

where D_{W0} is the uniform downwash and obtained by using the momentum theory as,

$$D_{W0} = \frac{C_{TA}}{2\mu_{TOT}} \tag{A.22}$$

where C_{TA} is the thrust coefficient and firstly estimated by using weight and μ_{TOT} total velocity at the shaft axes and represented as,

$$\mu_{TOT} = \sqrt{\mu_{XS} + \mu_{YS} + \lambda_0} \tag{A.23}$$

And λ_0 is uniform inflow ratio (normalized induced velocity) calculated with momentum theory as,

$$\lambda_0 = \mu_{ZS} - D_{W0} \tag{A.24}$$

D_{WC} and D_{WS} are cosine and sine component of downwash which,

$$D_{WC} = \frac{C_{MHA}}{\mu_{TOT}} \tag{A.25}$$

$$D_{WS} = \frac{C_{LHA}}{\mu_{TOT}} \tag{A.26}$$

where C_{MHA} and C_{LHA} are pitch moment and rolling moment coefficients added through the uniform downwash and firstly estimated by using momentum theory and weight again like thrust coefficient C_{TA}.

First estimations;

$$C_{TA} = \frac{mg}{\rho\pi\Omega^2 {R_T}^4} \tag{A.27}$$

$$C_{MHA} = \frac{mg\sin(\beta_{1C})Z_H}{\rho\pi\Omega^2 {R_T}^5} \tag{A.28}$$

$$C_{LHA} = \frac{mg\sin(\beta_{1S})Z_H}{\rho\pi\Omega^2 {R_T}^5} \tag{A.29}$$

Other steps of iteration;

$$C_{TA} = \frac{T_{HA}}{\rho\pi\Omega^2 {R_T}^4} \tag{A.30}$$

$$C_{MHA} = \frac{M_{HA}}{\rho\pi\Omega^2 {R_T}^5} \tag{A.31}$$

$$C_{LHA} = \frac{L_{HA}}{\rho\pi\Omega^2 {R_T}^5} \tag{A.32}$$

So K_{1X} and K_{1Y} which are Glauert downwash factors and calculated with equations below,

$$K_{1X} = \frac{\left(\sqrt{{\mu_{XS}}^2 + {\mu_{YS}}^2}\right)\mu_{XS}}{{\mu_{TOT}}^2} \tag{A.33}$$

$$K_{1Y} = \frac{\left(\sqrt{{\mu_{XS}}^2 + {\mu_{YS}}^2}\right)\mu_{YS}}{{\mu_{TOT}}^2} \tag{A.34}$$

The blade segment total velocity components are developed in three parts. Those indipendent of segment position, those dependent on segment position and interference effects made up of downwash. The velocities at the blade segments are obtained by transforming the fixed shaft vectors into the rotating hub axes system then transferring to the blade hinge position, transforming into blade span axes through the euler angles flapping "β" and lagging "δ" and finally transferring to the segment position on the blade. These total velocity components are used to calculate the resultant velocity, local mach number and local angle of attack. The local values are needed to be assigned for look-up table of blade airfoil aerodynamic coefficients (for C_l and C_d interpolation depends on mach number and angle of attack).

Total blade segment velocities in perpendicular direction will be,

$$U_{P_I} = U_{PA_{IB}} + \frac{y_{2_{IS}}}{\Omega_T}\left(U_{PB_{IB}}\right) + U_{PD_I} \tag{A.35}$$

where $I = 1,2, \ldots \ldots NSS * NBS$ total number of segments and $IB = 1,2, \ldots . NBS$

The first velocity component which is independent of segment position is,

$$\begin{aligned} U_{PA_{IB}} = & -\mu_{XS}\sin(\beta_{IB})\cos(\psi_{IB} + \delta_{IB}) \\ & + \mu_{YS}\sin(\beta_{IB})\sin(\psi_{IB} + \delta_{IB}) + \mu_{ZS}\cos(\beta_{IB}) \\ & + \frac{e}{\Omega_T}\{\cos(\beta_{IB})\left[q_s\cos(\psi_{IB}) + p_s\sin(\psi_{IB})\right] \\ & - \sin(\beta_{IB})\sin(\delta_{IB})\left(r_s - \Omega\right)\} \end{aligned} \tag{A.36}$$

And second velocity component which is dependent of segment position is,

$$U_{PB_{IB}} = -\dot{\beta}_{IB} + q_s\cos(\psi_{IB} + \delta_{IB}) + p_s\sin(\psi_{IB} + \delta_{IB}) \tag{A.37}$$

For tangential direction total segment velocities will be,

$$U_{T_I} = U_{TA_{IB}} + \frac{y_{2_{IS}}}{\Omega_T}\left(U_{TB_{IB}}\right) \tag{A.38}$$

$$U_{TA_{IB}} = \mu_{XS}\sin(\psi_{IB} + \delta_{IB}) + \mu_{YS}\cos(\psi_{IB} + \delta_{IB}) - \frac{e}{\Omega_T}[\cos(\delta_{IB})\,(r_s - \Omega)] \tag{A.39}$$

$$U_{TB_{IB}} = \dot{\delta}_{IB}\cos(\beta_{IB}) + \sin(\beta_{IB})\,[p_s\cos(\psi_{IB} + \delta_{IB}) - q_s\sin(\psi_{IB} + \delta_{IB})] - \cos(\delta_{IB})\,(r_s - \Omega) \tag{A.40}$$

Finally resultant velocity at the blade segment will be,

$$U_{Y_I} = \sqrt{{U_{T_I}}^2 + {U_{P_I}}^2} \tag{A.41}$$

And Mach number

$$M = U_{Y_I}\frac{\Omega_T R_T}{a} \tag{A.42}$$

where “a” is the speed of sound.

After obtaining the velocity components and by velocity terms determining the Mach number and angle of attack for look up table the aero data can be defined and interpolated.

Finally, the flapping dynamic equations should be added for obtaining Euler angles of main rotor. The flapping equation of motion of main rotor becomes,

$$
\begin{aligned}
\ddot{\beta}_{IB} = \frac{M_b}{I_b}\Big[\cos(\beta_{IB})\{\dot{W}_{SH} & \\
& + eR_T[2\Omega(p_s\cos(\psi_{IB}) - q_s\sin(\psi_{IB})) \\
& + \dot{p}_s\sin(\psi_{IB}) + \dot{q}_s\cos(\psi_{IB})]\} \\
& + \sin(\beta_{IB})\cos(\delta_{IB})\{\dot{V}_s\sin(\psi_{IB}) - \dot{U}_s\cos(\psi_{IB}) \\
& - e(r_s - \Omega)^2\}\Big] \\
& + \cos(\beta_{IB})^2\Big[\cos(\delta_{IB})\{\dot{p}_s\sin(\psi_{IB}) \\
& + \dot{q}_s\cos(\psi_{IB}) - 2(\dot{\delta}_{IB} \\
& + \Omega)(q_s\sin(\psi_{IB}) - p_s\cos(\psi_{IB}))\} \\
& - 2\Omega\sin(\delta_{IB})\,(p_s\sin(\psi_{IB}) - q_s\cos(\psi_{IB}))\Big] \\
& + \sin(\beta_{IB})\cos(\beta_{IB})\big[2\dot{\delta}_{IB}(r_s - \Omega) - (r_s - \Omega)^2\big] \\
& + \frac{M_{FAB_{IB}}}{I_b}
\end{aligned}
\tag{A.43}
$$

Under these circumstances total forces and moments about the hub fixed shaft axes becomes equations 2.1-2.6.

B. **Numerical Testing of Fixed-Point Iteration Method**

For hover condition, the results of limit values are given in the table below. The parameters are in degree unit. It can be seen in the last column that, how many iteration results are used for required condition.

λ	α_S	β_{1S}	β_{1C}	θ_{1S}	Iteration number
0.1	0	0	0	0	5
10	0	0	0	0	29
0.1	10	0	0	0	5
10	10	0	0	0	29
0.1	0	10	0	0	6
10	0	10	0	0	31
0.1	10	10	0	0	6
10	10	10	0	0	31
0.1	0	0	10	0	8
10	0	0	10	0	43
0.1	10	0	10	0	8
10	10	0	10	0	43
0.1	0	10	10	0	9
10	0	10	10	0	52
0.1	10	10	10	0	9
10	10	10	10	0	52
0.1	0	0	0	10	5
10	0	0	0	10	29
0.1	10	0	0	10	5
10	10	0	0	10	29
0.1	0	10	0	10	6
10	0	10	0	10	31
0.1	10	10	0	10	6
10	10	10	0	10	31
0.1	0	0	10	10	8
10	0	0	10	10	41
0.1	10	0	10	10	8
10	10	0	10	10	41
0.1	0	10	10	10	9
10	0	10	10	10	52
0.1	10	10	10	10	9
10	10	10	10	10	52

For 55 knots, the results of limit values are given in the table below.

λ	α_S	β_{1S}	β_{1C}	θ_{1S}	Iteration number
0.1	0	0	0	0	7
5	5	5	5	5	17
10	10	10	10	10	48

For 95 knots, the results of limit values are given in the table below.

λ	α_S	β_{1S}	β_{1C}	θ_{1S}	Iteration number
0.1	0	0	0	0	11
5	5	5	5	5	19
10	10	10	10	10	61